University of Montreal

Effect of charge-modifying coatings on the antibacterial effect of silver nanoparticles for *Escherichia coli*

By

Reinaldo Román Martín Pardo

Department of Chemistry, Faculty of Arts and Sciences

Thesis presented to obtain the master's degree in chemistry

September 2022

University of Montreal

Department of Chemistry, Faculty of Arts and Sciences

This thesis entitled

Effect of charge modifying coatings on the antibacterial effect of silver nanoparticles on *Escherichia coli*

Presented by

Reinaldo Román Martín Pardo

Has been evaluated by a jury composed by the following persons

Kevin James Wilkinson
Research Director

Patrick Hayes
Jury Member

Karen Waldron
Jury Member

Résumé

L'émergence de bactéries multirésistantes dues à une utilisation abusive d'antibiotiques est devenue l'une des menaces les plus dangereuses pour la santé publique. Le développement de nouveaux médicaments et la recherche d'agents antibactériens non traditionnels ont conduit à la nanotechnologie en tant que solution potentielle à ce problème. Les nanoparticules d'argent (NPs d'Ag) sont largement connues pour leur effet antibactérien. Cette étude vise à synthétiser des NPs d'Ag avec différents revêtements et à relier leurs propriétés physico-chimiques à leurs activités biocides, en mettant l'accent sur la façon dont leur charge de surface (estimée par leur potentiel zêta) affecte leurs efficacités antibactériennes et anti-biofilm. Les NPs d'Ag ont été synthétisées en utilisant du citrate comme agent de stabilisation et du polyvinylpyrrolidone, du polyéthylène glycol, de la chitosane et du polyéthylèneimine comme revêtements. La Spectroscopie de Masse à Plasma Inductif de Particule Unique, la Diffusion de Lumière Dynamique et les mesures de potentiel zêta ont été utilisées pour caractériser les NPs d'Ag préparées. La caractérisation des formulations de nanoparticules a montré qu'elles avaient des diamètres similaires d'environ 10 nm et des charges allant de -46 mV à 16 mV. Les comptages de plaques d'agar et les tests de micro dilution ont montré que les NPs d'Ag synthétisées étaient très efficaces pour empêcher la croissance des cellules bactériennes Escherichia coli. Des biofilms d'E. coli ont été cultivés et exposés aux NPs d'Ag, puis vérifiés à l'aide d'une microscopie à balayage laser confocal montrant que les formulations de NP avec un potentiel zêta négatif avaient plus d'activité anti-biofilm que les NP chargées neutres ou positives.

Mots-clés: nanoparticules d'argent, potentiel zeta, propriétés antibactériennes, biofilms, *Escherichia coli*.

Abstract

The emergence of multidrug resistant bacteria due to the misuse of antibiotics has become one of the most dangerous threats to public health. Development of new drugs and the search for non-traditional antibacterial agents have led to nanotechnology as a potential solution to this problem. Silver nanoparticles (Ag NPs) are widely known for their antibacterial effect. This study aims to synthesize Ag NPs with different coatings and relate their physicochemical properties with their biocidal activities, with special emphasis on how their surface charge (estimated via their zeta potential) affects their antibacterial and antibiofilm efficacies. Ag NPs were synthesized using citrate as a stabilizing agent and polyvinyl pyrrolidone, polyethylene glycol, chitosan and polyethyleneimine were used as coatings. Single Particle Inductively Coupled Plasma Mass Spectroscopy, Dynamic Light Scattering, and zeta potential measurements were used to characterize the prepared Ag NPs. Characterization of the nanoparticle formulations showed that they had similar diameters of around 10 nm and charges ranging from -46 mV to 16 mV. Agar Plate Counts and microdilution assays showed that the synthesized Ag NPs were very effective in preventing growth of *Escherichia coli* bacterial cells. *E. coli* biofilms were grown and exposed to the Ag NPs and checked afterwards with a confocal laser scanning microscopy showing that NP formulations with a negative zeta potential had more anti-biofilm activity than neutral or positive charged NPs.

Keywords: silver nanoparticles, zeta potential, anti-bacterial properties, biofilms, *Escherichia coli.*

Index

List of tables

List of figures

List of acronyms and abbreviations

Ag NPs: Silver nanoparticles

ATP: Adenosine Triphosphate

BHI: BBL^{TM} Brain Heart Infusion

CFU: Colony Forming Unit

Chi: Chitosan

Chitosan-Ag NPs: Chitosan coated silver nanoparticles

Cit: Citrate

Citrate-Ag NPs: Citrate stabilized silver nanoparticles

DLS: Dynamic Light Scattering

E. coli: *Escherichia coli*

EPM: Electrophoretic Mobility

FCS: Fluorescence Correlation Spectroscopy

MBC: Minimum Bactericidal Concentration

MIC: Minimum Inhibitory Concentration

NPs: Nanoparticles

OD: Optical Density

PEG: Polyethylene glycol

PEG-Ag NPs: Polyethylene glycol coated silver nanoparticles

PEI: Polyethyleneimine

PEI-Ag NPs: Polyethyleneimine coated silver nanoparticles

ppm; ppb; ppt: parts per million; parts per billion; parts per trillion

PVP: Polyvinylpyrrolidone

PVP-Ag NPs: Polyvinylpyrrolidone coated silver nanoparticles

ROS: Reactive Oxygen Species

SP-ICPMS: Single Particle Inductively Coupled Plasma Mass Spectroscopy

TFTC: Too Few to Count

TNTC: Too Numerous to Count

TSB: Bacto^{TM} Tryptic Soy Broth

To my family

Acknowledgements

I would like to express my gratitude to my research director, professor Wilkinson, for his supervision, his patience and for giving me this great opportunity. I would also like to thank Faraz, Ibrahim, Nesrine and Houssame for being very helpful and informative, as well as the rest of the research group for creating a nice work environment. Lastly, my parents for their support and concern, my sister-in-law for her words of encouragement, my wife for accompanying me through this journey and my brother for always being there for me.

Chapter 1 – Introduction

The overuse of antibiotics has led to an increase of infections where bacteria are resistant to antimicrobial treatments[1]. Indeed, the existence of multidrug resistant bacteria is one of the most important current threats to public health[2] and represents an emergency situation for immunocompromised people[1]. Antibiotic resistance may develop via multiple mechanisms such as alteration or inactivation of the antibiotic by the bacteria or a change in the metabolic pathway to avoid the disruptive effect of the antibiotic, amongst others[3]. This has led to a need for innovative and alternative treatments.

Nanoparticles (NPs) have emerged as a viable alternative to antibiotics and seem to have a high potential to solve the problem of multidrug resistant bacteria[4] as they rely on entirely different mechanisms of antibacterial activity than traditional antibiotics[3]. Silver ions are known for their strong biocidal effects and silver compounds have been used as disinfectants for a long time[5]. The antimicrobial properties of silver and their nanomaterials encourage its use in biomedical applications, water and air purification, food production, cosmetics, clothing and numerous household products[6]. Silver nanoparticles may be released into the environment as waste of industrial production, erosion of engineered materials in household products and from washing or disposal of items that contain silver nanoparticles. Widespread use of silver nanoparticles may be harmful for the environment in the long run[6], so there is an interest in developing new non-traditional antibacterial agents based on silver nanoparticles with high efficacy. Consequently, several studies have examined the role of silver nanoparticles as antibacterial agents[4, 6-11], and looked at how their physicochemical properties may influence their effectiveness[10, 12-15].

1.1 Bacteria

Bacteria are simple unicellular organisms with no nuclear membrane, mitochondria, Golgi bodies or endoplasmic reticulum[16]. A bacterial cell is surrounded by a cell membrane made of phospholipids which keeps nutrients, proteins and the rest of the components of the cytoplasm

inside the cell[17]. Cell division is managed by a cytoskeleton[18] comprised of several structural filaments. Being that they have no internal membranes, biochemical reactions related to energy and metabolism occur across the cell membrane due to concentration gradients[19]. The genetic material of bacteria is a single bacterial chromosome of DNA in the nucleoid, located in the cytoplasm[20].

The size of bacteria is usually in the order of a micrometer. They are present in most habitats on Earth, including extreme environments such as acidic hot springs or radioactive waste[21]. It has been estimated that the vast majority of bacterial species have not been completely identified[22]. They are carried by humans and animals alike and most bacteria present in the human body are harmless and even essential for life[23]. However, some bacteria are pathogenic and can cause infectious diseases with fatal consequences in certain cases. Bacterial disease can result from the toxic effects of bacterial products like toxins or when bacteria invade normally sterile body tissues and fluids[16]. Antibiotics used to treat bacterial infections are classified as *bactericidal* if they kill the bacteria or *bacteriostatic* if they prevent their growth.

Bacteria are either gram-positive cells with a thick peptidoglycan layer as a cell wall, or a gram-negative with a thin peptidoglycan layer and an overlying outer membrane[16]. These differences in structure can influence their susceptibility to antibiotics or affect the efficacity of some medications[24].

Cell division occurs by means of binary fission (asexual reproduction) after the bacteria grow to a fixed size. This process can be so fast that some bacterial populations can double in 17 minutes under the right conditions[19]. Bacterial growth typically spans over 4 phases:

1- Lag phase: a phase of slow growth while cells adapt to a high nutrient environment;
2- Logarithmic phase: a phase of quick exponential growth in which the nutrients are metabolized as fast as possible;
3- Stationary phase: the growth is limited by depleted nutrients; the metabolic activity is reduced, and non-essential cellular proteins are consumed;
4- Death phase: when the bacteria run out of nutrients and die.

Asexual organisms like bacteria produce offspring with identical genomes and are clonal. But errors during the replication of DNA or exposure to mutagens can produce mutations to their genetic material and cause the bacteria to evolve[25].

1.1.1 Biofilms

Bacteria often attach to surfaces and form dense heteroaggregates with exopolymers called biofilms[23]. Biofilms are communities of microorganisms embedded within a self-produced matrix of extracellular polymeric substance[4]. Most bacteria found in natural environments like soils or associated with living organisms are bound to surfaces in biofilms[26].

Biofilms are often present during chronic bacterial infections or in infected implanted medical devices, which is problematic as bacteria that are embedded within biofilms are much harder to kill[27]. In fact, biofilms may be one of the reasons we see more chronic diseases instead of acute-phase diseases[4].

The biofilm matrix production is controlled by enzymes that are secreted when nutrients are available[27]. A rapid formation is promoted by presence of a suitable surface and higher concentration of substances like calcium salts, polyamines, extracellular iron, and bile salts[28, 29] . The structure of the forming biofilm will depend on the nutrients available, the accumulation of waste products and other factors such as cell growth and death[28]. Several species of bacteria can detect and respond to cell population density by regulating the expression of specific genes, a process named quorum sensing. Proteins involved in this mechanism are called quorum sensing molecules. A chemical signal, by means of a quorum sensing molecule, is responsible for the transition from floating separated cells to an aggregated state that is precursor of the biofilm (Figure 1).

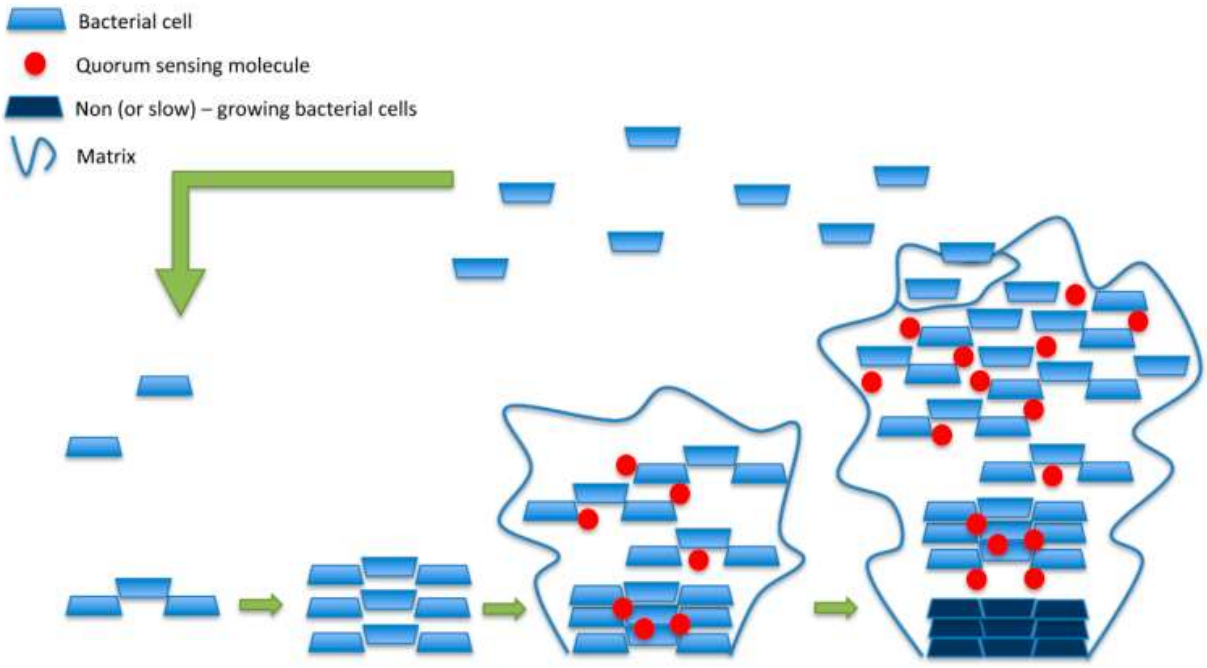

Figure 1. Formation of a biofilm. Separated bacterial cells floating in a liquid support send a chemical signal that induces surrounding cells to aggregate[4].

The structure of biofilms makes the bacteria within more resistant to antimicrobial agents, mainly through one or several mechanisms such as[27]:

1- Delaying the penetration of the agent through the matrix
2- Altering the growth rate of the organisms in the biofilm
3- Other physiological changes caused by the mode of growth of the biofilm

Escherichia coli (E. coli) is one of the most common biofilm-forming bacteria associated with human infections[4].

1.2 Silver Nanoparticles

Silver has been widely used since antiquity as a therapeutic agent for many diseases[7]. Before the beginning of antibiotics therapy, silver was already known for its antiseptic activity and was used in the treatment of open wounds and burn patients[7, 30].

For inherently antibacterial materials like silver, an increase in the surface to volume ratio results in an enhancement of the antibacterial effect. Nanoparticles allow for a greater interaction with the surrounding environment, meaning more interaction with bacterial surfaces, therefore they are ideal for antimicrobial applications[3].

Silver nanoparticles have extended use in the field of medicine and therapeutics[7, 9]. They have been shown to be very effective against bacteria[4, 6], fungi[31] and viruses[32]. Studies using strains of multi-drug resistant bacteria have also shown promising results[33]. The formation of bacterial biofilms has been shown to be inhibited through the use of silver nanoparticles, which render the organism unable to synthesize the exopolysaccharides that make up the biofilm matrix[34].

1.2.1 Mechanism of antibacterial action

While the antibacterial properties of Ag NPs have been widely studied, their mechanism of action is still a point of discussion and is further complicated by the fact that different organisms interact differently with these nanoparticles[4].

Physicochemical characteristics of the nanoparticles such as size, surface properties and shape affect biological processes like circulation, biodistribution, cellular internalization and trafficking[15]. Smaller nanoparticles seem to have a superior ability to penetrate bacterial outer membranes and cell walls[4].

Among the mechanisms of action that have been proposed to explain the antibacterial properties of NPs are alteration of cell wall, cytoplasm, membrane, inhibition of respiratory activity, inhibition of DNA replication or modification of intracellular adenosine triphosphate (ATP) levels[4]. The three most common mechanisms proposed in literature are (Figure 2):

- Disruption of ATP production and DNA replication by silver ions;
- Generation of reactive oxygen species (ROS) catalyzed by silver nanoparticles and silver ions in presence of oxygen;
- Damage to cell membranes by silver nanoparticles.

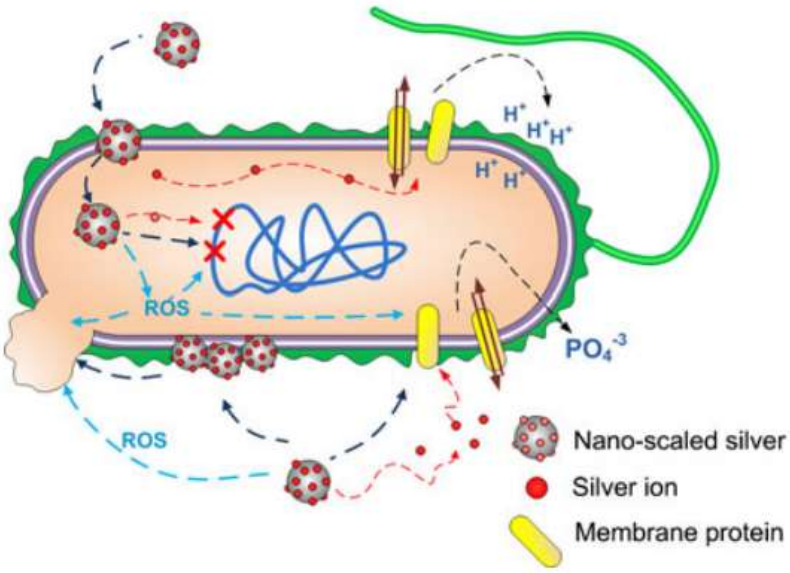

Figure 2.- Diagram summarizing interactions of silver nanoparticles and silver ions with the bacteria[6]. Silver nanoparticles release silver ions which in presence of oxygen, catalyze the generation of ROS. Accumulation of nanoparticles in the membrane affecting its permeability. Damage to ATP production and DNA replication.

When nanoparticles dissolve, they generate silver ions. *In vivo*, the release of silver ions is thought to occur, mainly as a product of reactions with H_2O_2[35] :

$$2\ Ag + H_2O_2 + 2\ H^+ \rightarrow 2\ Ag^+ + 2\ H_2O$$

These ions are expected to be partly responsible for the antibacterial properties of silver nanoparticles as they interact with enzymes in the respiratory chain and disrupt synthesis of ATP. They also bind to membrane proteins, causing the collapse of proton motive force leading to proton leakage[36]. Other cellular processes disrupted by ionic silver include inhibition of phosphate uptake and an increase in DNA mutations during polymerase chain reactions[6].

Reactive oxygen species (ROS) can be formed during regular metabolism of the bacterial cell. An excess of these species results in free radicals that attack the lipids of the cellular membrane. Silver nanoparticles in the presence of oxygen catalyzes the generation of ROS, resulting in the subsequent damage to the biological organism[37]. Such damage includes a breakdown of the membrane, loss of mitochondrial function or DNA damage.

Silver nanoparticles also appear to be able to penetrate the cell through the bacterial membrane, creating "pits", resulting in increased permeability and an incapability to regulate transport through the plasma membrane[37, 38]. These pits and gaps in the membrane result in a leakage of reducing sugars and proteins and inactive respiratory chain dehydrogenases, and in general, the structure of the bacterial membrane becomes damaged[39].

These effects are more evident for nanoparticles with smaller sizes and a positive zeta potential. Due to the electrostatic forces between positively charged nanoparticles and the negative surface of bacteria, a stronger attraction is present, leading to greater interaction and an increased possibility of penetration of the bacterial membranes[4, 6]. However, a study on the effects of negatively charged silver nanoparticles on *E. coli* showed that despite their negative surface charge, the nanoparticles could interact with the bacterial membrane and this could cause structural changes, degradation, leading to cell death [38].

Gram-negative bacteria like *E. coli* contain porins, which are water filled channels in their outer membrane. The presence of these porins facilitates transport of silver ions and their penetration, and strains of *E. coli* that are deficient in porins are found to be more resistant to the action of silver ions[40].

1.3 Physicochemical properties of colloids

Dispersed systems are characterized by being composed by more than one phase. Typically, we have a disperse phase and a dispersion medium if the system is comprised of two phases. Colloids are a suspension of particles (disperse phase) of between 1 nm to 1 µm of diameter, in a dispersion medium. They are a metastable system in which the particles are large enough to have supramolecular structure and properties, while being sufficiently small to not sediment quickly[41].

1.3.1 Zeta potential (ζ)

The interface that separates a fluid attached to the surface of a particle from a mobile fluid, is called the slip plane. Zeta potential (ζ) is the electrical potential measured at the location of this plane and it is the net electrical at the slip plane (Figure 3). It is often used in the literature to quantify the magnitude of the charge of a nanoparticle, though strictly speaking it is a measure of potential and not charge, because it can be negative or positive depending on the chemical composition of the particle.

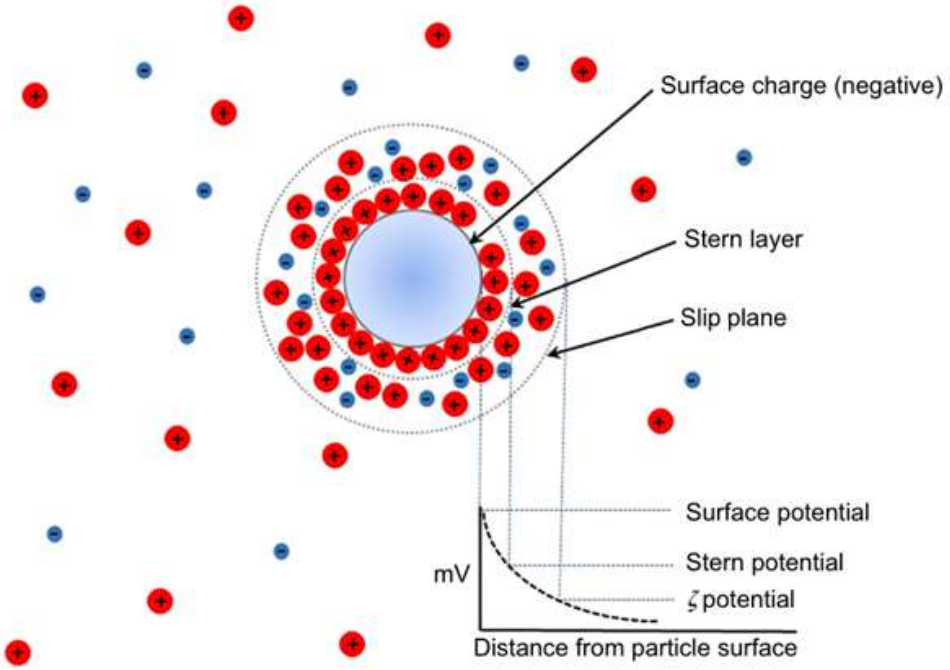

Figure 3.- Zeta potential is the electric potential at the slip plane and is different to the Stern potential or the surface potential as those are defined at different locations[42]. The image shows an example of a particle and displays at which location is measured each potential.

In a colloidal system, dispersed particles present two layers of charged ions with opposite charges. The Stern layer can be found close to the surface and consists of ions strongly bound. The Diffuse layer consists of ions loosely bound, and at its edge with the surrounding liquid we can find the slip plane, in which the zeta potential is defined. These two layers are collectively referred as the electric double-layer[42]. Ions within the diffuse layer travel with a particle as it moves because of their strong attraction to the particle.

Under the influence of an electric field, charged particles will move towards the electrode that has a charge opposite to that of the nanoparticle. A common method to calculate ζ Potential is through electrophoretic mobility or EPM, which is the velocity at which these particles travel under the influence of an applied electrical field E:

$$\mu_e = \frac{\nu}{E} \quad \textit{(Equation 1)}$$

where E is the electrical field; ν is the velocity of the particle and μ_e is the electrophoretic mobility.

We can find the zeta potential using the Helmholtz-Smoluchowski equation:

$$\zeta = \frac{4\pi\eta}{\varepsilon} f(\kappa a)\mu_e \quad \textit{(Equation 2)}$$

where η is the viscosity of the medium; ε is the dielectric constant of the solvent and $f(\kappa a)$ is Henry's function, where a is the particle radius and κ is the inverse of the Debye screening length, often taken as a measure of the thickness of the electrical double layer. Then, κa is the ratio of particle radius to double layer thickness.

Two limits are often applied to Henry's function: The Huckel approximation ($f(\kappa a) = 1.0$ for $\kappa a < 1$) if the Debye screening length is significant or the Smoluchowski approximation ($f(\kappa a) = 1.5$ for $\kappa a > 100$) if the Debye screening length is considered negligible. The Smoluchowski model fits systems with large disperse particles or polar media with a high dielectric constant, such as aqueous media.

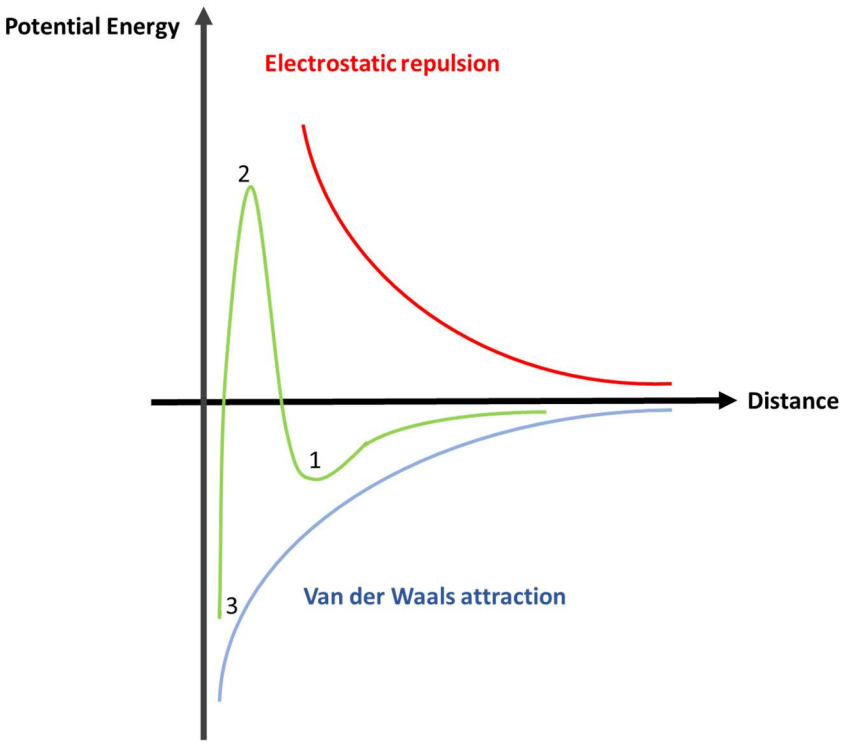

Figure 4.- DLVO theory explains the stability of colloidal systems by combining two curves of electrostatic repulsion and van der Waals attraction. The potential energy profile shows how when particles come closer, they go through 1: minimum potential energy (shallow minimum), 2: potential barrier (maximum) and 3: deep well minimum.

The stability of a colloidal suspension depends on the balance between two forces: electrostatic repulsion between particles and van der Waals attraction. This theory is known as DLVO (named after Derjaguin, Landau, Verwey and Overbeek). The total potential energy is the sum of the attraction potential and the repulsion potential (Figure 4). Outside of the double layer, the potential is close to zero. As two particles approach each other, their electrical double layers begin to interfere, and electrostatic repulsion increases[43]. At the same time, the van der Waals attraction also increases. The potential energy goes through a shallow minimum before finding a maximum when the particles are about to touch. This maximum represents an energy barrier and at closer distances than it, the combination of forces results in a deep attractive well of potential energy. At the maximum, repulsion is still greater than attraction and the particles remain dispersed in the medium. However, if the energy barrier is overcome, particles aggregate and be trapped together by van der Waals forces. In this state, attractive forces are higher than repulsive ones and particles irreversibly coagulate. Stable colloids can't reach this state due to

the energy barrier and they stay in the shallow minimum, where they may form weak attractions and are easily dispersed[44]. As such, the height of the maximum is representative of how stable a colloidal system is.

In a suspension of nanoparticles, a high surface charge will often lead to a stable colloidal dispersion due to electrostatic repulsion. On the other hand, if the charge is small enough, the repulsion can be exceeded by attractive forces and lead to aggregation. Zeta potential are thus used to predict the stability of a colloidal dispersion and the tendency to aggregation[45]. Similarly, particle charge will greatly influence particle interactions in suspensions of multiple particle types (heterocoagulation) or particle-surface interactions.

Zeta potential is often reported with the pH of the medium and ionic strength as this can be an important factor when performing the measurement. On the particle's surface, H_3O^+ can cause a buildup of positive charges while OH^- ions will cause it for negative charges. If there are functional groups present at the surface, they could also be affected by the solution's pH as they become protonated or deprotonated. These events may alter the zeta potential value.

The physicochemical ***properties of nanoparticles*** can determine their cellular uptake, biodistribution and interaction with biological surfaces [13]. Surface charge is especially known to affect the fate of nanoparticles in biological systems. As such, they can influence the mechanism in which nanoparticles interact with bacteria. Coatings added to nanoparticles can lead to a shift in zeta potential regardless of original surface charge. Both positively and negatively charged molecules can be efficiently internalized into a cell, via interactions with charged proteins present on the cell membrane[46, 47]. Cellular uptake has been correlated with the absolute value of surface charge[48], making surface modification of polymer-nanoparticle systems a common way to control internalization. Internalization is preceded by the binding of nanoparticles on the cell membrane, a step affected by surface charge. Cellular surfaces are dominated by highly anionic proteoglycans that have mostly ionic interactions with positively charged NP shells. Higher surface charge causes a strong binding to the cell membrane and a higher cellular uptake. However other studies show a higher cellular uptake for nanoparticles with a negative charge compared to positive or less negative surface charge[49]. A possible explanation is the existence of

a few cationic sites for adsorption of negatively charged particles. Formulation of nanoparticles with different surface properties can influence the mechanism of cellular uptake (pinocytosis, non-specific or receptor mediated endocytosis, phagocytosis) as well as their subsequent intracellular distribution and localization into specific targets (lysosomes, mitochondria, cytoplasm)[50]. As such, the magnitude of zeta potential plays a major role in some targeted therapies and on the properties of nano-drug delivery systems[50].

1.3.2 Other factors that affect colloid stability

Colloid stability is the capacity of a colloidal system to avoid separation of their phases in relatively long period of time. It can also be interpreted as the capability to avoid aggregation of the dispersed particles, as aggregates large enough in size could cause sedimentation. Surface modification with citrate imposes a relatively high negative charge in the nanomaterials, decreasing the chance of homoaggregation of nanoparticles by collision.

As discussed before, surface coatings play a major role in stabilization by modification of zeta potential. When the surface of a nanoparticle is covered by an adsorbed layer of polymers, a phenomenon called steric stabilization can be produced. This consists of the polymer acting as a steric impediment preventing the particles from getting close enough to be in range of attractive forces. The thickness required for this to happen must be such that it exceeds the Debye layer.

Heteroaggregation from interaction between nanoparticles and free polymers present in solution (excess from coating agents added) can lead to sedimentation but is a slow process. The occurrence of large enough aggregates is most likely a product of collision of two aggregates instead of addition of single colloids to an existing aggregate[41]. As such, high temperatures that lead to faster particle movement cause an increase in the number of collisions and the probability of aggregation. For this reason, nanoparticles are preferably stored at low temperatures.

Charged polymers used for coatings can have their structure affected by the acidity of the medium. Consequently, the charge of the molecule and the magnitude of zeta potential of the coated nanoparticle are dependent on the pH of the solution. Isoelectric point is defined as the pH at which a molecule carries no net electrical charge. The further away the pH is from the

isoelectric point, the higher the absolute value of the charge should be as well as the repulsion between charged colloids, leading to higher stability.

1.4 Single Particle Inductively Coupled Plasma Mass Spectrometry

Inductively Coupled Plasma Mass Spectrometry (ICPMS) is a type of mass spectrometry in which samples (usually in liquid state) are introduced into an instrument via a nebulization system that produces an aerosol of polydisperse droplets. With the use of an inductively coupled plasma the solvent evaporates, and the solid particles are atomized and ionized. Ions enter the quadrupole of the mass spectrometer where they are separated according to their mass/charge ratio. ICPMS is considered as a fast and versatile elemental analysis technique, that can provide multielement analysis and with low detection limits[51].

Single Particle Inductively Coupled Plasma Mass Spectrometry (SP-ICPMS) is a specific technique of ICPMS in which the measurements are performed on a particle-by-particle basis. For sufficiently dilute suspensions of nanoparticles, their passage through the plasma will yield small ion packets of a duration of 300-600 µs that result from the vaporization, atomization, and ionization of each nanoparticle. SP-ICPMS relies on the assumption that each recorded pulse corresponds to a single nanoparticle. The number concentration of NPs can be determined from the frequency of the pulses, whereas the intensity of each pulse is proportional to the mass of the element.

The mass concentration (C) can be found from:

$$C = \frac{R}{\eta Q K_{ICPMS}} \frac{M}{A N_A} \quad \textit{(Equation 3)}$$

where R is the signal intensity (number of ions counted per time unit); η is the nebulization efficiency; Q is the sample uptake rate; K_{ICPMS} is the detection efficiency (ratio of ions detected vs atoms introduced into the ICPMS); A is the atomic abundance of the isotope ^{107}Ag; N_A is the Avogadro constant and M is the atomic mass of silver.

If the suspension is sufficiently diluted that just one NP is detected per reading, the frequency of NPs detected (f) will be:

$$f = \eta Q N \quad \textit{(Equation 4)}$$

where N is the NP number concentration.

Sizes or diameters are found by calibration with a NP standard of the same element, and using:

$$d = \sqrt[3]{\frac{6r}{\pi \rho \chi K_{ICPMS} 6} \frac{M}{A N_A}} \quad \textit{(Equation 5)}$$

where d is the diameter or size of the nanoparticle assuming a spherical NP. In the non-spherical case, the size represents the diameter of a sphere who would occupy the same volume as our NP. r is the signal intensity for a single reading in which each reading represents a NP; ρ is the density of the NPs and χ is the mass fraction of silver in the NP.

1.5 Dynamic Light Scattering

To determine the size distribution of a suspension of nanoparticles, a technique called Dynamic Light Scattering (DLS) is frequently used. A monochromatic light source, such as a laser, passes through a polarizer into the sample. Molecules hit by the light diffract it in all directions, causing a constructive interference that will result in light regions called speckles. The light becomes scattered (Rayleigh scattering) when passing through the sample, then it goes through another polarizer and is finally collected by a photomultiplier. The resulting image is known as a speckle pattern. Several repetitions produce a set of speckle patterns, which can be analyzed by an autocorrelator. As the particles diffuse in time, the conditions for constructive interference change and the speckles move[52].

The particles in suspension move randomly (Brownian motion), causing the scattering intensity to fluctuate over time as the distance between the scatterers (molecules hit by light) is constantly changing. The intensity fluctuation gives information about the movement of the particles over

time. Samples must be filtered or centrifuged to remove any dust that could affect the patterns obtained.

Scattered intensity can give information about the shape or structure of the scattering objects, which is the basis of other light or X-ray experiments. However, in DLS the information comes from the time-variant contribution of the scattered intensity. For this a time-averaged intensity-intensity correlation function, also called autocorrelation function must be considered.

In order to compute the autocorrelation function, the scattered electric fields are considered first:

$$g^{(1)}(q,\tau) = \frac{\langle E(q,0)E(q,\tau)\rangle}{\langle I(q,0)\rangle} \quad \textit{(Equation 6)}$$

where:

$g^{(1)}(q,\tau)$ is the autocorrelation function of the scattered electric fields, also called as the first order correlation function or intermediate scattering function. Angular brackets denote the expected value operator, the weighted average of all possible outcomes of a random variable with a finite number of outcomes. q is the scattering vector; τ is the delay time; $\langle I(q,0)\rangle$ is the intensity at time zero; $E(q,0)$ is the scattered electric field at time zero and $E(q,\tau)$ at time = τ.

A second order autocorrelation function or normalized intensity autocorrelation function is defined as:

$$g^{(2)}(q,\tau) = \frac{\langle I(q,0)\rangle I(q,\tau)}{\langle I(q,0)^2\rangle} \quad \textit{(Equation 7)}$$

where $g^{(2)}(q,\tau)$ represents the intensity autocorrelation function and $I(q,\tau)$ represents the intensity after the delay time.

The two functions are related by the Siegert relation:

$$g^{(2)}(q,\tau) = 1 + (g^{(1)}(q,\tau))^2 \quad \textit{(Equation 8)}$$

which is the main result obtained through the DLS measurements, and contains the information used for size determination[53]. Sizes determined in DLS are referred to as hydrodynamic diameters (and hydrodynamic radii can be derived from it), because they are generally larger than the true

sizes obtained from static measurements. Is used synonymously with the Stokes radius, which is the radius of a hard sphere that diffuse at the same rate as the solute. This radius includes water molecules dragged by the particle as it moves through the solution.

Sizes are not measured directly, but rather via their diffusion constants. The diffusion coefficient of non-interacting spherical particles dispersed in a solvent is given by the Stokes-Einstein equation:

$$D = \frac{k_B T}{\xi} \quad \textit{(Equation 9)}$$

where D is the translational diffusion coefficient, k_B is Boltzmann constant, T the temperature in Kelvin and ξ is the friction coefficient that a sphere of hydrodynamic radius R_H experiences in a medium of viscosity η according to:

$$\xi = 6\pi\eta R_H \quad \textit{(Equation 10)}$$

The Stokes-Einstein relation is also known as the generalized fluctuation-dissipation theorem. The field-correlation function can be simplified to:

$$g^{(1)}(q,\tau) = e^{-q^2 D\tau} \textit{ (Equation 11)}$$

Equation 9 and 10 are substituted into equation 11:

$$g^{(1)}(q,\tau) = e^{-q^2 \frac{k_B T}{6\pi\eta R_H}\tau} \textit{ (Equation 12)}$$

which can be related to the autocorrelation function of the scattered electric fields by the Siegert relation (Equation 8).

1.6 Confocal Laser Scanning Microscopy

Confocal Laser Scanning Microscopy (CSLM) is a technique that achieves a higher resolution and contrast compared to a conventional microscope. Its main difference revolves around the use of a pinhole to block the out-of-focus light. Both use light to excite the sample and detect the resulting fluorescence, but instead of exciting all parts of the sample at the same time, CSLM uses

point illumination. This allows it to eliminate out-of-focus signals. However, this comes at a cost in signal intensity, and long exposures are required. The detector is usually a photomultiplier tube or an avalanche photodiode, and the signal (current) is transformed into an electrical one (voltage).

The technique allows the creation of 3D images. Using the point illumination and oscillating mirrors, the light beam can scan across the sample in the horizontal plane. Images obtained can be used to create a 3D image or a 2D image of the z axis.

Being a non-invasive technique, it can be used to study live organisms such as bacteria. Typically, a dye is used to make selected bio-organisms visible. To study anti-bacterial agents, a combination of dyes is used to distinguish living bacteria from dead ones.

1.6.1 Fluorescence Correlation Spectroscopy

Fluorescence correlation spectroscopy (FCS) is a technique used to quantify molecular dynamics, and commonly utilized to measure diffusion coefficients of biomolecules. FCS sensitivity can be up to the single molecular level. Molecules are fluorescently labeled and diffused through a focused light, the resulting fluorescence fluctuations are observed, and their time correlation is analyzed. A confocal microscope with a pinhole system for point illumination is also used in this technique with the same advantage of eliminating out-of-focus signals.

Like DLS, the diffusion pattern creates an intensity fluctuation, and an autocorrelation function can be used for computation purposes. The data acquisition is similar to that of DLS (explained in Section 2.5), and the same procedure can be used to obtain the diffusion coefficient and hydrodynamic radius via the Stokes-Einstein Equation (Equation 9). Compared to DLS, FCS is better for small particles and the use of a dye can improve the results in a complex system. More importantly, it allows the mapping of diffusion coefficients of nanoparticles within bacterial biofilms.

1.7 Previous studies

Surface properties of the Ag NPs have a crucial impact on their potency, as they influence important physical (aggregation, affinity for bacterial membranes) and chemical (oxidative dissolution, formation of a passivating layer) phenomena[10]. First, the bactericidal action of the Ag NPs is highly correlated to their surface reactivity and their specific surface area, which is the total surface area of a solid material per unit of mass (typically expressed in m^2/g). A larger number of atoms on the surface means that more of them are available to interact with bacteria or release ions. Smaller nanoparticles with a higher specific surface will have a higher dissolution rate and greater interactions with bacteria and therefore, enhanced antibacterial properties[6]. Aggregation can hinder the activity of antibacterial systems[10], and nanoparticles with a high stability will form fewer aggregates that would reduce their surface area and impact negatively their antibacterial properties[6]. Certain particle shapes, such as decahedral, also encourage bactericidal activity as they contain larger densities of atom in facets, meaning that more atoms are available for interactions[11].

A study of silver nanoparticles synthesized with a range of 5 to 100 nm of diameter, showed that smaller nanoparticles were the most effective against several strains of bacteria[54]. Particularly, *E. coli* was found to be very sensitive to Ag NPs size. Nanoparticles with less than 10 nm had their antibacterial efficacy significantly enhanced. Another study that explores the effect of size, performs the synthesis of Ag NPs at different pH values to evaluate the effect on stability[12]. It was observed that at more acidic pH, the nanoparticles were more stable, less prone to aggregation and smaller. These nanoparticles were found to have more antimicrobial activity as well. A similar conclusion was found when the toxicity of Ag NPs of different sizes was evaluated on bacteria[11, 55], yeast, algae, and other biological systems[8, 55].

Several articles have been written about the surface properties of silver nanoparticles, specifically their surface charge[10, 56, 57]. The addition of coating agents is one of the most common ways to modify the surface charge. Ethylhexyl sulfosuccinate[57], bovine serum albumin[57], polyethylene glycol (PEG)[58] are examples of negative charge coatings, while poly(L-lysine)[57],

cetyltrimethylammonium bromide[57], branch polyethyleneimine (PEI) [14, 58, 59] and chitosan[60] are used as positive coatings. Citrate stabilized Ag NPs also result in a negative surface charge[14, 56, 57, 61]. Polyvinylpyrrolidone (PVP)[14, 57-59], Brij 35[57] and Tween 20[57] are uncharged molecules typically used as neutral coatings. A study of the effect of charge modifying coatings on the toxicity of silver nanoparticles against *bacillus* species (Gram positive), found a direct correlation with surface charge[14]. Negative Ag NPs were the least toxic whereas the positively charged NPs were the most toxic. While this study explores a wide range of charge values, positive and negative, it didn't evaluate if the nanoparticles would exhibit the same behavior against Gram-negative bacteria such as *E. coli*.

Silver nanoparticles have also been tested for their potential anti-biofilm activity, with promising results[34]. While there have been studies that prove that Ag NPs can be effective against bacterial biofilms[62, 63], limited research has been conducted on how their efficacy is affected by physicochemical properties.

While silver nanomaterials are very promising as antibacterial agents, their effects on higher organisms and the environment can be harmful if their use becomes too widespread, prompting the need for research on their safe and more effective use[6]. In recent years, growing attention has been placed on the green synthesis of these nanoparticles using biological reducing and capping agents like algae, fungi, bacteria, and plant extracts. These synthesis methods bring numerous advantages to the environmental and economic aspects of the production of silver nanoparticles [33].

The effect of size and surface charge on the antibacterial properties of silver nanoparticles have been extensively studied[64]. However, to the best of our knowledge there isn't a comparative study of the anti-biofilm properties of Ag NPs synthesized by the same method with different surface charge values. As such, the objective of this study is to:

- Synthesize several novel Ag NPs with different coatings and determine how the addition of coating agents influences the physical properties of the Ag NPs.
- Relate the physical and chemical composition of the Ag NPs to their ability to kill bacteria, specifically *Escherichia coli,* a Gram-negative bacterium.

- Determine how the Ag NPs coatings affect their effectiveness against bacterial biofilms.

Chapter 2 – Methods

2.1 Bacteria

A strain of *E. coli* (ATCC 25922) bacteria previously stored at -80°C was used in this study. Before any experiment, a new batch was grown by thawing the frozen *E. coli* (letting it rest around 10 min at room temperature) and subsequently adding 10 µL of the bacteria and 20 µL of glucose (previously prepared by dissolving 8 g of glucose in 20 mL of water) to 10 mL of culture medium, and left to grow overnight at 37°C.

2.1.1 Culture medium preparation

Bacto™ Tryptic Soy Broth (TSB) was used as the culture medium for most experiments. TSB consists of 17 g/L of casein pancreatic digestate, 3 g/L of soy papaic digestate, 2.5 g/L of dextrose, 5 g/L of sodium chloride and 2.5 g/L of dipotassium phosphate. To prepare the culture medium, 15 g of TSB was dissolved in 500 mL of water.

Alternatively, BBL™ Brain Heart Infusion (BHI) was used in a complementary experiment to find the Minimum Inhibitory Concentration (MIC). BHI composition consists of 6 g/L of brain heart infusion, 6 g/L of peptic digestion of animal tissue, 14.5 g/L of gelatin pancreatic digestion, 3 g/L of dextrose, 5 g/L of sodium chloride and 2.5 g/L of disodium phosphate.

2.1.2 Optical Density Measurement

To check the optical density (OD) of a bacterium, a DR 2800 spectrophotometer (HACH) was used. The OD was measured at a single wavelength of 600 nm, using the same culture medium that was used to grow the bacteria (TSB in most cases) as the blank. In cases where the OD was above the desired value (1 or 0.1 depending on the experiment), the bacteria were diluted in broth until desired value was reached.

2.2 Synthesis of Nanoparticles

The nanoparticles were synthesized as follows[65]:

Solutions of 0.5 M citric acid and 2.5 mM tannic acid were prepared. 1 mL of each solution was added to 97 mL of Milli-Q Water. The resulting solution was heated while stirring until boiling. At this point the heating was stopped and 1 mL of a 25.0 mM silver nitrate solution was added. At that moment the solution was composed of 5.0 mM citric acid, 0.025 mM tannic acid, 0.25 mM silver nitrate and water. The solution was stirred while cooling.

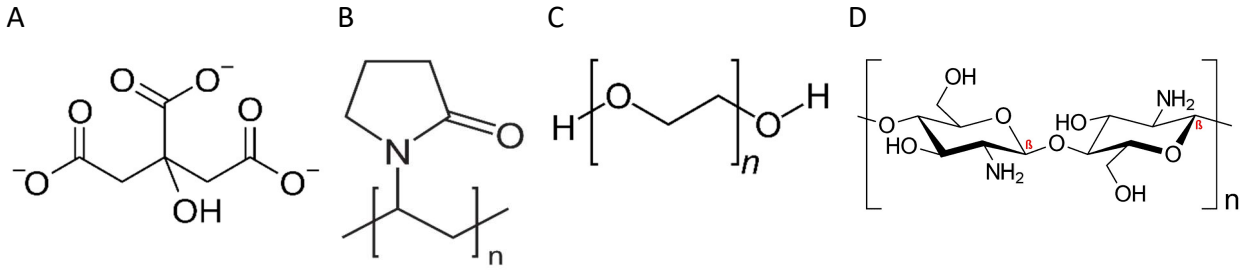

Figure 5.- Structure of the molecules used as coating. A: citrate anion; B: PVP; C: PEG; D: chitosan

The synthesized citrate coated Ag NPs before were left to rest overnight before adding several nanoparticle coatings used to adjust the particle charge: 40 kDa PVP solution, 4 kDa PEG, 190 kDa chitosan and 25 kDa PEI (Figure 5). Stock solutions of the coating agents (10% w/w PVP, 10% w/w PEG, 0.02% w/w chitosan and 10% w/w PEI) were added individually to the citrate coated nanoparticles[66] 100 µL at a time, while stirring, with 15 min intervals between each addition. For PVP, PEG and PEI, three formulations were prepared for each polymer: 300 µL, 600 µL and 900 µL added to 20 mL of the citrate-Ag NPs. As a result, Ag NPs with 1.5 mg/mL, 3 mg/mL, and 4.5 mg/mL concentrations of each of the three coatings were obtained. Due to its viscosity and quick agglomeration, as shown by the UV spectra, chitosan was added in 50 µL intervals to prepare three formulations: 100 µL, 300 µL and 500 µL chitosan added to 20 mL of citrate-Ag NPs. The final concentrations were 1 µg/mL, 3 µg/mL, and 5 µg/mL of chitosan. Formulations were stored at 4º C, never frozen. Before being used in an experiment, they were first shaken and then put in an ultrasonic bath (Branson 5510) for 15 minutes to reduce agglomeration.

Citric acid (ACS reagent, ≥99,5%), tannic acid (ACS reagent), silver nitrate (ACS reagent, ≥99,0%), PEI (branched, M_w 25 kDa), PVP (M_w 40 kDa), PEG (for synthesis, M_w 4 kDa), and chitosan (medium molecular weight, M_w 190 kDa) were purchased from Sigma Aldrich through Millipore Sigma.

2.3 Molecular Absorbance Spectroscopy

Molecular Absorbance Spectroscopy spectra were acquired with a Thermo Fisher Evolution 201 UV-Visible Spectrometer from 300 to 900 nm with a 0.5 nm interval. Polystyrene Thermo Scientific™ Sterilin™ cuvettes with 1 cm path length and a 1 mL capacity were used. Each measurement was made using 100 µL of sample and adding 900 µL of Milli-Q water.

2.4 Single Particle ICPMS

Measurements of particle numbers and Ag^+ concentrations were performed using an ATTOM ES magnetic sector ICP MS from Nu Instruments. Samples were diluted 500 000 times in water total in three stages: two consecutive 100x dilutions and a 50 times dilution; a vortex shaker was used before and after every dilution. The final concentration of Ag NPs was expected to be around 50 parts per trillion (ng/L).

To detect total Ag concentrations, nanoparticles were digested in nitric acid. First, 300 µL of sample were diluted in 3 mL of a solution of nitric acid in water (1% w/w). Then a 5 times dilution and two consecutive 100 times dilution were performed to reach a final concentration around 50 parts per trillion of Ag NPs (ng/L).

2.5 DLS and Zeta Potential

Dynamic light scattering was performed on a Mobius EPM analyzer (Wyatt) to obtain the hydrodynamic radius of Ag NPs. The same equipment was used to obtain the zeta potential of the samples. Calculations and data collection were performed using the software Dynamics 7.8.1.3 that operates within the Mobius instrument. A zeta potential transfer standard of $\zeta = 40.0 \pm 5.8$ mV was used as the standard for zeta potential measurements. For every sample measured, its pH was reported using a OAKLON pH Meter 510 series. A Thermo Scientific ORION 8165 BNWP Ross Sure Flow pH electrode was used. When an experiment required prior centrifugation, these were performed in a Multifuge 1 S-R Heraeus with a SORVALL Heraeus 75002002 G module (18.7 cm of radius).

2.6 Agar Plate Counts

To measure the bactericidal properties of the formulations, the method of Agar Plate Counts was used. A strain of *E. coli* was grown overnight at 37°C in presence of TSB culture medium and glucose. The next day, prior to use, the optical density (OD) of the bacteria was measured at 600 nm and adjusted to 1 via dilution, if needed.

100 µL of the bacteria with OD = 1 were added to a vial with 900 µL of sample (coated Ag NPs) or 900 µL of culture medium for the negative control or 900 µL of ethanol for the positive control. After 1 min (or 5 min in a separate experiment), 100 µL of the resulting solution was dissolved in 900 µL of NaCl (0.85% w/w) aqueous solution (Tube 1). This process was repeated four more times (Tubes 2-5). 100 µL from each of the tubes were evenly spread over separate agar plates and these agar plates were stored at 37°C overnight.

After 24 hours, agar plates are inspected, and the Colony Forming Units (CFU) are counted. The optimal amount of CFU for comparison between samples is expected to be between 30 and 300, higher being deemed too numerous to count (TNTC) and lower too few to count (TFTC). Reduction percent is calculated as:

$$R = 100 * \frac{X - X_{min}}{X_{max} + X_{min}} \quad \textit{(Equation 12)}$$

where R is the reduction percent; X is the amount of CFU following exposure to the Ag NPs ; X_{min} is the CFU in the negative control and X_{max} is the CFU following exposure to the positive control.

2.7 Microdilution assays

Two properties can be measured to characterize the antibacterial properties of nanoparticles or any drug or chemical with potential bactericidal activity: Minimum Inhibitory Concentration (MIC) is the lowest concentration that prevents visible growth of bacteria; Minimum Bactericidal Concentration (MBC) is the minimum concentration of an antibacterial agent that results in bacterial death. Assays to determine these two properties are often used to compare the efficacy of several antibacterial agents against the same bacterium[40, 54, 60].

To determine the MIC, a technique known as broth microdilution assay was performed. A 96 well cell culture plate was used for the microdilution assays. The first well of each row contained 180 µL of Ag NP sample, and each well along the row had half of the concentration (diluted in TSB Broth) of the previous well. This was done by adding 180 µL of broth to all wells except the ones in the first column, then adding 180 µL of sample, mixing it well and taking 180 µL of the resulting solution and adding it to the next well across the row. This methodology is repeated for each well until the end of the row (Figure 6). For the negative control, a row with 180 µL of TSB Broth is used in each well. For the positive control, a row with 180 µL of ethanol (in each well) was used. Bacteria were grown overnight and then diluted to an OD = 0.1. Twenty (20) µL of the 0.1 optical density bacteria are added to each well of the cell culture plate prepared previously, which was stored at 37°C overnight. In this manner, we have the same number of bacteria exposed to a range of dilutions of the bactericidal agents.

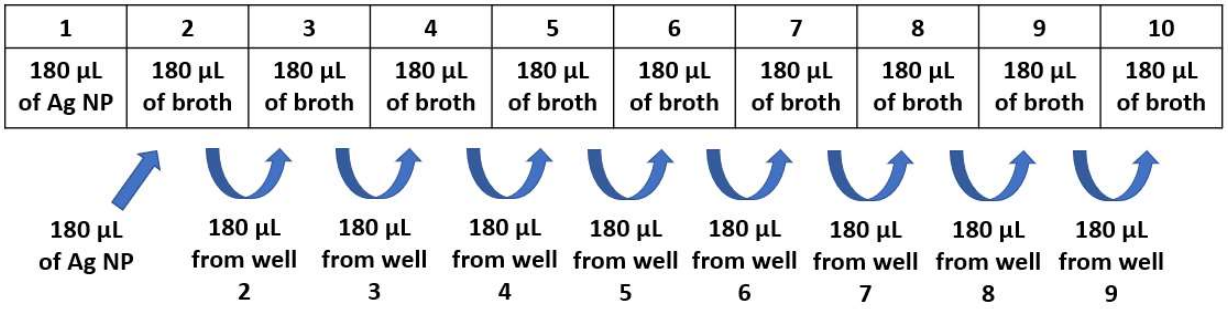

Figure 6.- Representation of a row in a 96 well plate used for broth microdilution assay. The first well in a row contains 180 µL of Ag NP sample while the rest contains 180 µL of broth. 180 µL is added to the second well, mixed, and then 180 µL of its content is added to the next well. The process is repeated across the row.

To determine the MBC, 100 µL of the well solutions from previous broth microdilution assays with equal concentration to MIC or lower, were taken and spread over an Agar Plate, then left overnight at 37°C. Wells with a lower concentration are expected to show fewer Colony Forming Units (CFU), if any, when spread over an agar plate. The highest concentration of Ag NP that results in no CFU will then be the MBC, as this is the lowest concentration of the antibacterial agent (Ag NP) required to kill the bacteria completely.

2.8 Biofilms

For biofilm essays, *E. coli* was incubated in TSB broth and glucose for 24 hours at 37°C. One hundred (100) µL of the bacteria from day 1 was diluted in TSB broth with 50 µL of glucose. Four hundred (400) µL of the resulting solution was added to an 8 well coverslip where it was incubated for 24 hours at 37 ^{o}C. On the third day, the solutions were removed from the wells and 400 µL of the Ag NPs formulations were added to each well for 1 min (or 5 min in a separate experiment), then carefully removed by pipette. Subsequently, 200 µL of BacLight^{TM} (Live/Dead^{TM} Bacterial Viability Kit) (a drop of Syto9 and propidium iodide in 1 ml of 0.85% NaCl) was added to each well and they were left in the dark for 20 min. The supernatant is again removed, and the wells were cleaned with 400 µL of NaCl, which was later removed. For the negative control, only

the BacLight™ was added (and the NP step was skipped). For positive control, ethanol was added instead of the NPs.

The slides with the biofilms were inspected on a Leica TCS SP5 microscope, using a 488nm/20mW Ar ion laser and an HCX PL APO 63x/1.20W objective. Conditions were constant for all the formulations between the experiments, using a smart gain of 835.0 V and a pinhole of 60.64 µm. Images taken by the confocal microscope are separated into 2 channels: red and green, which were channels corresponding to the wavelengths emitted by fluorophores of the Baclight™ assay. Propidium Iodide emitted red fluorescence corresponding to the dead cells, while the green fluorescence of the Syto9 was an indicative of living cells.

The percentage of dead cells were calculated from:

$$\frac{N_D}{N_D+N_A} * 100 \quad \textit{(Equation 13)}$$

where N_A is the number of live bacteria and N_D is the number of dead bacteria.

Bacterial numbers were deemed to be proportional to the intensity of the green (live) or red (dead) channels of the microscopic images. An alternative method was used, using the pixel count instead of the intensity, and results were exactly the same.

Two sets of experiments (with 5 replicates each) were performed, one for the 1 min exposure and another for 5 min exposure. To compare results between the two sets of experiments, reduction percents compared to the values of positive and negative controls were calculated. For this, the negative control was taken as the minimum, the positive control was taken as the maximum and the reduction percent of each sample was rescaled according to the equation:

$$R = 100 * \frac{X-X_{min}}{X_{max}+X_{min}} \quad \textit{(Equation 14)}$$

where R is the reduction percent; X is the percentage of dead cells following exposure to the sample; X_{min} is the percentage of dead cells in the negative control and X_{max} is the percentage of dead cells following exposure to the positive control.

2.8.1 Diffusion experiments

Experiments to compare the diffusion of the different Ag NPs formulations through biofilm were planned. A preliminary study was performed on formulations with rhodamine 110 as a dye, but the concentration of rhodamine used was too high and the resulting images were too intense. Later experiments with other dyes or different rhodamine concentration were not performed due to technical limitations (equipment malfunction) and were temporarily abandoned. More detailed research is being done in the research group in collaboration with a different author, Houssame-Eddine Ahabchane, using the same formulations, a new microscope, and several bacteria (including *E. coli*). These experiments are being performed presently.

Chapter 3 – Results and Discussion

3.1 Synthesis of Nanoparticles and Absorption Spectroscopy

The coating agents were selected to include differently charged coatings, in order to determine how they would influence the bactericidal properties of the nanoparticles. Given that the size of the nanoparticles plays an important role in their activity[13, 15] it was necessary to ensure that the core nanoparticles were all close in size with each other. Size was controlled using a method[65] to synthesize core citrate coated nanoparticles. This core nanoparticle was subsequently used to synthesize the different charged formulations[66], with the only property changing from one particle to another being the coating. The citrate-coated, core nanoparticles should be negatively charged[14, 56, 57]. PVP was selected as a neutral coating[14, 57]; PEG as a strongly negative charged coating[58]; and chitosan as a positively charged coating[60] (Figure 5). The isoelectric point of PEG is around 2.5 making the deprotonated form the prevalent one and remaining negatively charged at all but the most acidic of pH ranges.

UV-vis measurements were used as a quick method to detect the maximum amount of coating that could be added without causing agglomeration. Every time 100 µL of coating was added to the citrate-Ag NPs, its UV-vis spectrum was measured and then compared by superposition to the original citrate-Ag NPs (Figure 7 and Figure 8). If no significant differences in the peak form or position were found, then it was assumed that no agglomeration took place. This way, it was found that the addition of 900 µL of coating agents (10% in weight) to 20 mL of the base citrate-Ag NPs were the limit conditions as further additions caused agglomeration. Three formulations (300 µL, 600 µL and 900 µL of coating agents added, resulting in 1.5 mg/mL, 3 mg/mL and 4.5 mg/mL concentrations respectively) with each of the coatings (PVP, PEG, PEI) were synthesized in order to vary the particle properties.

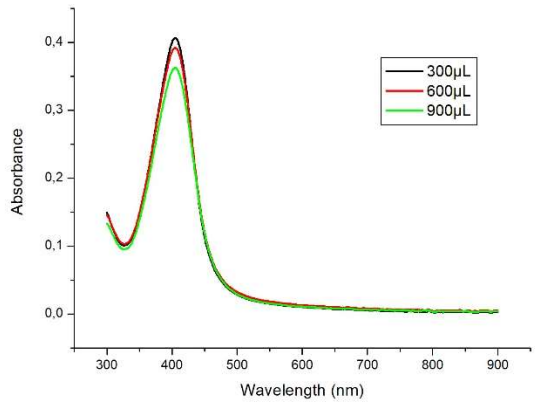

Figure 7.- Comparison between the spectra of Ag NPs after adding 300 µL, 600 µL and 900 µL of 10% w/w PVP 40k.

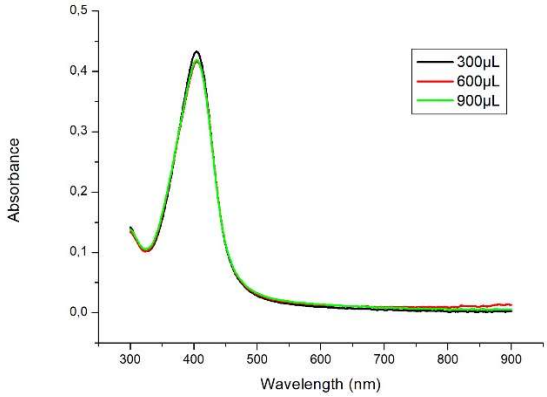

Figure 8.- Comparison between the spectra of Ag NPs after adding 300 µL, 600 µL and 900 µL of 6% w/w PEG 4k.

On the other hand, for the additions of chitosan, the absorption results showed agglomeration, even for relatively lower amounts of added chitosan (Figure 9). For that reason, the chitosan stock solution that was used had to be diluted to 0.02 % w/w and the amounts of coating agents added were reduced to 100 µL, 300 µL and 500 µL (Figure 10).

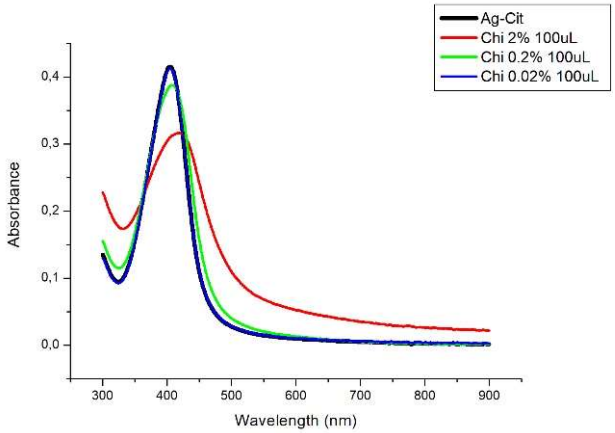

Figure 9.- Comparison between the initial citrate-AgNPs and AgNPs obtained after adding 100 µL of chitosan with different concentrations.

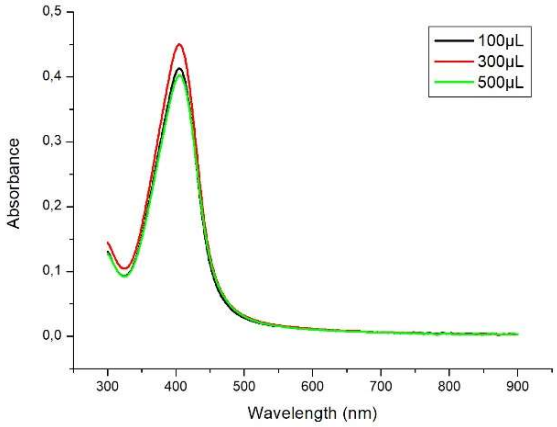

Figure 10.- Comparison between the spectra obtained for Ag NPs after adding 100 µL, 300 µL and 500 µL of 0.02% chitosan.

UV-vis spectroscopy was also used to check for agglomeration one month after the synthesis, by measuring the NPs 30 days after preparation to identify differences between spectra (Figure 11).

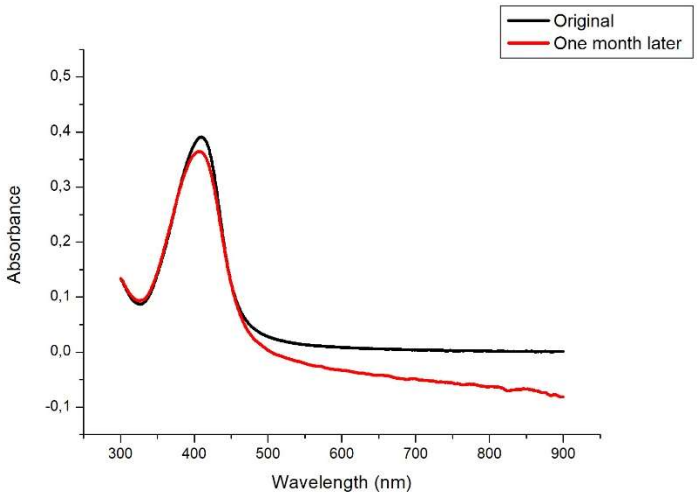

Figure 11.- Comparison between the UV-Vis spectra of citrate-Ag NPs in water immediately after synthesis and after one month stored at room temperature

Similarities between the peaks of the two spectra suggested that our citrate-Ag NPs remained stable over the course of a month. Silver nanoparticles are known to aggregate over long periods of time[67] and this may affect their biological activites[61]. For this reason is good practice to redisperse the nanoparticles before any measurement, using vortex shaking and ultrasound .

3.2 Single Particle ICPMS and DLS

Single Particle ICPMS was used to verify the sizes of the nanoparticles (Table 1). As can be seen, the particle sizes (diameters) were relatively similar and in the range of 9 to 10 nm (4.5 to 5 nm of radius). The only exception is 3 mg/mL PEG–Ag NPs with a slightly larger size, with no real explanation for what caused this other than manipulation error during the synthesis. The variance in radius with other formulations is less than 1 nm and may not cause a significant difference on antibacterial efficacy. Standard errors are obtained by dividing the sample standard deviation by the root of the number of measurements.

Table 1.- Physical Radii of AgNPs samples measured by SP-ICPMS. Obtained by assuming a particle density for the Ag of 10.49 g cm^{-3} and under the assumption that they are spheres. Standard error values are provided.

Coating	Particle radius (nm) N=3
citrate-Ag NPs	4.9 ± 0.1
1.5 mg/mL PVP-Ag NPs	4.6 ± 0.1
3 mg/mL PVP-Ag NPs	4.8 ± 0.1
4.5 mg/mL PVP-Ag NPs	5.0 ± 0.1
1.5 mg/mL PEG-Ag NPs	4.9 ± 0.1
3 mg/mL PEG-Ag NPs	5.5 ± 0.1
4.5 mg/mL PEG-Ag NPs	4.6 ± 0.1
1 µg/mL Chi-Ag NPs	4.6 ± 0.1
3 µg/mL Chi-Ag NPs	4.7 ± 0.1
5 µg/mL Chi-Ag NPs	4.6 ± 0.1

Other results extracted from the SP-ICPMS studies include particle number concentration, mass concentration of the nanoparticles and mass concentration of the dissolved silver (Table 2). The theoretical concentration of silver from the synthesis was around 25 mg/L; as described in the Methods, a 500 000x dilution was performed in SP ICPMS to get the concentration of the sample to around 50 ng/L. Results are presented as measured by the instrument and then corrected for the dilution by multiplying by 500 000.

Table 2.- Number concentration of Ag NPs, mass concentration of Ag NPs and mass concentration of dissolved Ag as measured by ICPMS. Samples were measured after dilution of the stock solutions by 500 000 times. For the mass concentration of Ag NPs and mass concentration of dissolved Ag, a calculation was made to find the concentrations in the original stock solutions. Standard error values are provided. Bar graphs of these results are shown in Figures A21-A23 in Appendix A.3.

Coating	Number concentration (Ag NPs/mL)	Mass concentration of Ag NPs		Mass concentration of dissolved Ag	
	Diluted samples	Diluted samples (ng/L)	Undiluted samples (mg/L)	Diluted samples (ng/L)	Undiluted samples (mg/L)
citrate-Ag NPs	(219 ± 5) x 10^3	1.54 ± 0.05	3.08	3.17 ± 0.01	6.34
1.5 mg/mL PVP-Ag NPs	(39 ± 1) x 10^3	0.21 ± 0.02	0.42	1.05 ± 0.10	2.10
3 mg/mL PVP-Ag NPs	(29 ± 1) x 10^3	0.20 ± 0.03	0.40	1.27 ± 0.06	2.54
4.5 mg/mL PVP-Ag NPs	(27 ± 2) x 10^3	0.23 ± 0.02	0.46	1.43 ± 0.07	2.86
1.5 mg/mL PEG-Ag NPs	(37 ± 2) x 10^3	0.26 ± 0.02	0.52	1.39 ± 0.01	2.78
3 mg/mL PEG-Ag NPs	(124 ± 4) x 10^3	1.89 ± 0.16	3.78	1.77 ± 0.07	3.44
4.5 mg/mL PEG-Ag NPs	(170 ± 4) x 10^3	0.96 ± 0.06	1.92	1.94 ± 0.06	3.88
1 µg/mL chitosan-Ag NPs	(203 ± 5) x 10^3	0.86 ± 0.11	1.72	1.86 ± 0.04	3.72
3 µg/mL chitosan-Ag NPs	(132 ± 5) x 10^3	0.66 ± 0.02	1.32	1.47 ± 0.07	2.94
5 µg/mL chitosan-Ag NPs	(78 ± 2) x 10^3	0.38 ± 0.01	0.76	1.44 ± 0.01	2.88

With respect to the citrate stabilized Ag NPs, we saw a drop in the number concentration of AgNPs for all of the formulations, especially the PVP coated, 1.5 mg/mL PEG-Ag NPs and 5 µg/mL chitosan-Ag NPs. In general, the results were inconsistent for number concentrations, with PEG coated particles showing higher concentrations with higher amounts of coating and chitosan showing the opposite effect. A similar trend could be seen for the mass concentration values, with the exception of 3 mg/mL PEG-Ag NPs having a higher mass concentration than citrate-Ag NPs. Furthermore, for all of the formulations, the mass concentrations are too low, considering

the theoretical yield was expected around 26 mg/L, suggesting that adsorptive losses might be occuring to the ICP-MS. The results for the mass concentrations for dissolved Ag are very low as well and don't account for the missing silver. Another possible explanation is that the diameter of the nanoparticles are too small and outside the detection limit of the equipment. Size distributions (Figure 12) show that most of the particles are between 8 and 10 nm in size (4 to 5 nm of radius), which is very close to the size detection limit of the equipment (7 nm of diameter), so it is probable that there are particles that are too small to be detected.

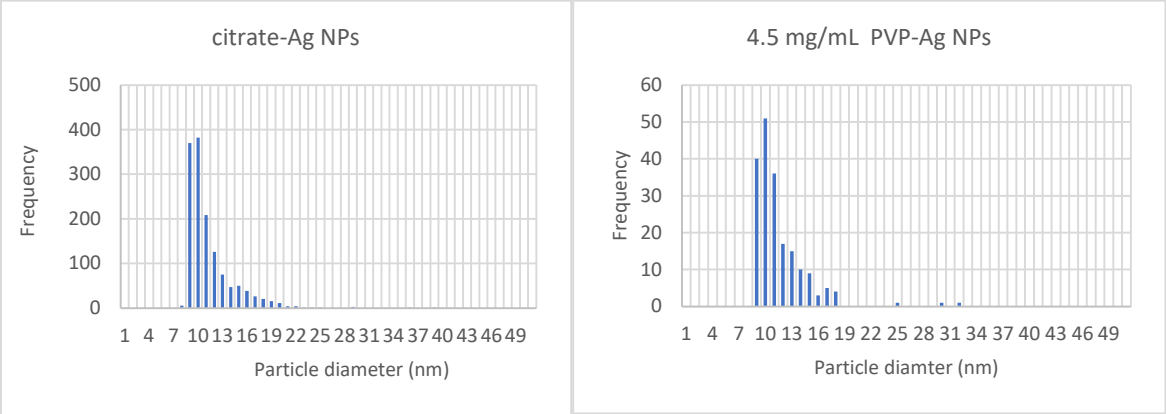

Figure 12.- Size distributions obtained using SP ICPMS for samples with citrate stabilization or 4.5 mg/mL PVP-Ag NPs coatings. The size distributions for the rest of the nanoparticles can be found in the Appendix A2 (Figures A20). The steep drop off at lower sizes (shark fin shape) suggests that we were close to the size detection limits of the instrument.

To check the actual silver concentration of the samples, an acid digestion was performed and subsequently ICPMS was performed on the digested samples. From these measurements, calculations were done to find the original silver concentration of the stock Ag NP solutions (Table 3), multiplying by 500 000 which was the factor of dilution. Results from digestion are closer to the theoretical yield for the synthesis, showing that there was a large loss of nanoparticles in the SP ICPMS measurements before digestion. Formulations have concentrations around 40 mg/L which is higher than the expected concentration (26 mg/L) from the theoretical calculations. In the case of citrate-Ag NPs (30 mg/L) this could be explained by manipulation errors while weighing the reagents or evaporation of the solvent during synthesis. The rest of formulations had considerably higher concentrations, which could happen because they were synthesized by adding coating to the previous citrate-Ag NPs, meaning that the errors are carried over from the

previous step and added to any manipulation error or solvent evaporation that occurs in this step.

Table 3.- Results of acid digestion of Ag NPs samples. Measurements correspond to a 500 000x dilution of the stock solution. Afterwards, the original concentration is calculated from these results. Bar graphs of these results are shown in Figures A24 in Appendix A.3.

Coating	Mass concentration of dissolved Ag	
	Measurements of diluted samples (ng/L)	Stock solution concentration (mg/L)
citrate-Ag NPs	60.6 ± 0.3	30.3
1.5 mg/mL PVP-Ag NPs	75.3 ± 0.4	37.6
3 mg/mL PVP-Ag NPs	87.8 ± 0.4	43.9
4.5 mg/mL PVP-Ag NPs	79.6 ± 0.5	39.8
1.5 mg/mL PEG-Ag NPs	76.4 ± 0.2	38.2
3 mg/mL PEG-Ag NPs	80.2 ± 0.4	40.1
4.5 mg/mL PEG-Ag NPs	78.7 ± 0.3	39.3
1 µg/mL chitosan-Ag NPs	97.4 ± 0.2	48.7
3 µg/mL chitosan-Ag NPs	95.0 ± 0.2	47.5
5 µg/mL chitosan-Ag NPs	81.2 ± 0.8	40.6

Hydrodynamic radii were measured by dynamic light scattering (DLS). In contrast to SP-ICP-MS, DLS detects the size of the core plus its particle coating and the electric double layer. While the particle radii measured by SP-ICPMS was around 4-5 nm, we can see that the hydrodynamic radii is considerably larger (Figure 13). Indeed, we can see a growing trend when adding more coating for PVP and chitosan coated NPs. PEG formulations did not seem to induce as many changes as a function of the amount of added coating.

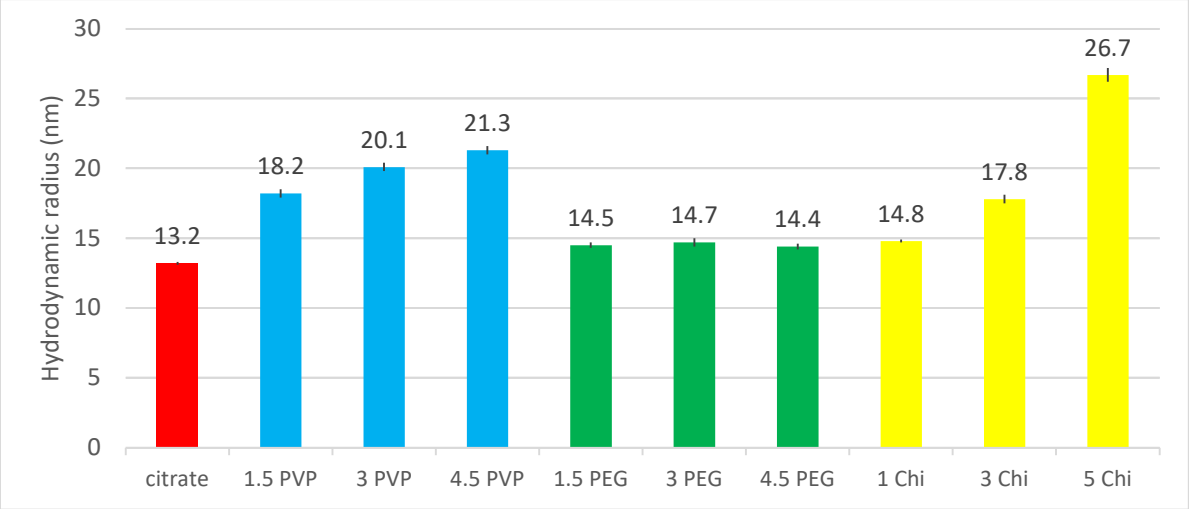

Figure 13.- Hydrodynamic radii of Ag NPs measured by DLS. Samples were diluted by a factor of 10 before measurements. Formulations with the same coating but different amount of coating, have the same bar color to better display the trends. Formulations are named according to the concentration of the coating in mg/mL (µg/mL in the case of chitosan). Chi refers to chitosan.

3.3 Zeta potential and pH

Citrate and PEG are known to provide a negatively charged surface, while a PVP coating should be neutral and chitosan should give a positive surface. Zeta potential measurements were made to corroborate that our formulations had the expected behaviour. The pH of the medium is known to strongly affect the value of zeta potential[12], and for this reason, it was determined before the zeta potential measurements (Table 4). The pH values show no major difference between formulations, as they were all in the range of 6.6 to 6.8. Citrate and PEG modified surfaces gave the NP negative values of zeta potential. PVP, despite being a neutral coating, resulted in Ag NP with negative values of zeta potential, that trended towards neutral with additional coating. This phenomen is not unexpected as PVP coated AgNPs are widely reported in literature with a slightly negative charge[14, 57]. A potential explanation is that excess anions from the synthesis like citrate, tannate or nitrate were adsorbed next to the PVP surface coating[57].

The chitosan coated NP should have been positively charged, however, the zeta potential of the chitosan-AgNPs wasn't reflecting this expectation. This may have been due to the low amount of chitosan that was used. Similar to above, the very negative value of the coating could have been due to the citrate anions in the media adsorbing to the chitosan coating at the surface of the NPs. This could also explain the observation that the chitosan-AgNPs had an increasing hydrodynamic radius. Being that one of our objectives was to attain a positively charged AgNP, new formulations with higher amounts of chitosan were explored.

Table 4.- Zeta potentials and pH measurements of the AgNP formulations. Zeta potential was calculated by the Smoluchowski Model. Six repetitions of the measurements were performed. Bar graphs of these results are shown in Figures A25 in Appendix A.4.

Coating	ζ Potential (mV) (N=6)	pH
citrate-Ag NPs	-24.6 ± 1.2	6.8 ± 0.2
1.5 mg/mL PVP-Ag NPs	-15.7 ± 0.7	6.7 ± 0.1
3 mg/mL PVP-Ag NPs	-11.0 ± 0.5	6.7 ± 0.1
4.5 mg/mL PVP-Ag NPs	-7.1 ± 0.3	6.6 ± 0.1
1.5 mg/mL PEG-Ag NPs	-38.3 ± 1.0	6.8 ± 0.1
3 mg/mL PEG-Ag NPs	-42.8 ± 0.9	6.8 ± 0.1
4.5 mg/mL PEG-Ag NPs	-46.2 ± 0.7	6.8 ± 0.2
1 µg/mL chitosan-Ag NPs	-26.1 ± 1.1	6.7 ± 0.3
3 µg/mL chitosan-Ag NPs	-39.7 ± 0.7	6.8 ± 0.1
5 µg/mL chitosan-Ag NPs	-42.4 ± 0.4	6.8 ± 0.1

As discussed above, when synthesizing the original chitosan formulations, a study was performed to find the maximum amount of coating that could be added without causing agglomeration. In

this study, 500 µL of 0.02% w/w chitosan was seen as the limit that could be added to 20 mL of the citrate-Ag NP core. In order to verify if the lack of a positive ζ potential could be related to the amount of chitosan being too low, a new formulation with double the amount of chitosan was synthesized by adding 1000 µL of 0.02% w/w chitosan to 20 mL of citrate stabilized nanoparticles. The result was a chitosan coating concentration of 10 µg/mL.

Even with higher added amounts of chitosan, negative zeta potentials of -33.2 ± 0.6 mV were determined. Furthermore, DLS measurements gave a radius of 1500 ± 300 nm. This meant that we were having severe agglomeration, and most likely formulations with even higher amounts of chitosan would have shown similar results and not have been usable in the study. In a further exploratory study, an even higher amount of chitosan was added, in order to see whether a positive zeta potential could be achieved and to eliminate the possibility of other problems with the coating itself. This time 5 mL of 0.2% w/w chitosan was added and the result was a coating concentration of 4 mg/mL.

For this formulation, measured zeta potentials were 43.0 ± 0.7 mV, showing that with higher concentrations of chitosan, a positively charged nanoparticle could be obtained. However, as expected, the DLS measurement gave a very large hydrodynamic radius of 1420 ± 60 nm, suggesting once again that severe agglomeration was affecting the viability of this formulation for our study. Given these results, we decided to explore other coatings that could result in a positively charged nanoparticle, such as PEI (Figure 14).

Figure 14.- Structure of PEI, the polymer used as coating with the intention to yield positively charged nanoparticles.

Using the exact same method as the previous NPs, three new formulations of PEI[59] coated nanoparticles were synthesized. While these formulations had slightly positive ζ potential, the values were much smaller than what was reported in literature. The hydrodynamic radii (Table

5) suggested that there was some limited agglomeration. Furthermore, pH values were higher than the rest of the formulations.

Table 5.- Zeta potentials, pH and hydrodynamic radii of the new formulations of PEI coated Ag NP. Six repetitions of the measurements were performed.

Coating	ζ potential (mV) (N=6)	pH	Hydrodynamic radius (nm)
1.5 mg/mL PEI-Ag NPs	3.0 ± 0.2	9.89	41.1 ± 0.7
3 mg/mL PEI-Ag NPs	3.2 ± 0.2	10.30	39.2 ± 0.8
4.5 mg/mL PEI-Ag NPs	2.5 ± 0.2	10.31	36.1 ± 1.3

A possible parameter affecting the zeta potential value, could be the presence of leftover reagents from the synthesis. Therefore, centrifugal ultrafiltration was explored as a possible means to purify the NP. Samples were loaded into Amicon® Ultra-15 centrifugal filter tubes and subsequently subjected to centrifugation at 4000 rpm (3345 G) in 4 periods of 1 hour. The filter was then washed in an ultrasound and the nanoparticles were redispersed in Milli-Q Water. The zeta potential of the NP was measured again after centrifugation (Table 6), to determine if there was a significant difference after purification. Since the values of zeta potential didn't change significantly after centrifugation for any of the particles, it doesn't appear that the excess citrate or tannic acid in solution was responsible for the unexpected zeta potential values. At the moment of synthesis these anions could have been strongly adsorbed and they are unable to be removed by centrifugation.

Table 6.- Comparison of zeta potential measurements of the formulations with the highest amount of coating, measured before and after centrifugation.

Coating	Before Centrifugation ζ Potential (mV)	After Centrifugation ζ Potential (mV)
4.5 mg/mL PVP-Ag NPs	-7.1 ± 0.3	-6.9 ± 0.5

4.5 mg/mL PEG-Ag NPs	-46.2 ± 0.7	-45.3 ± 0.9
5 µg/mL chitosan-Ag NPs	-42.4 ± 0.4	-44 ± 5
4.5 mg/mL PEI-Ag NPs	2.5 ± 0.2	3.1 ± 0.2

Another reason worth exploring was the effect of agglomeration. As seen by DLS, the PEI formulations showed some agglomeration. They also had a more basic pH than the rest of the NP. Branched PEI has three pKa values depending on the degree of substitution of the amines: primary amines have a value of 4.5, secondary amines have a value of 6.7 and tertiary amines have a value of 11.6[68]. From the pH values measured previously for PEI coated nanoparticles, we could infer that PEI has a low level of protonation which would explain the low positive charge. The addition of acid could fix this and at the same time lead to some deagglomeration. Therefore, drops of diluted HCl were added to PEI samples until the pH attained 7.0 (Table 7) closer to the rest of Ag NPs formulations.

Table 7.- Zeta potential, pH and hydrodynamic radii of the new formulations with PEI coated Ag NP after adding HCl to adjust the pH closer to 7. Six repetitions of the measurements were performed.

Coating	**Zeta potential (mV) (N=6)**	**pH**	**Radius (nm)**
1.5 mg/mL PEI-Ag NPs	8.9 ± 0.9	6.90	25.7 ± 0.6
3 mg/mL PEI-Ag NPs	12.2 ± 0.3	6.91	24.3 ± 0.7
4.5 mg/mL PEI-Ag NPs	16.1 ± 0.4	6.89	21.1 ± 0.7

These results showed that agglomeration accounted for the difference in hydrodynamic radii between the PEI coated NPs and the initial formulations. The pH modification also resulted in a more positive zeta potential because they are now close to the second pKa of PEI. A study of the

effect of pH on the charge and protonation level of PEI found that at pH close to 7 there is an inflexion point from weakly charged to highly charged for this polymer[69].

Therefore we can use these new formulations in subsequent tests with *E. coli* bacteria as they provide cationic coated Ag NPs to compare with the neutral and anionic NPs. Previously we had attained Ag NPs with various degrees of negative zeta potential and now we can also explore how the addition of a coating that provides a positive charge will influence the bactericidal properties of the silver nanoparticles.

3.4 Agar Plate Counts

Agar Plate counts tests were used to check for the bactericidal properties of the formulations. Bacteria was exposed to each formulation for 1 min before adding NaCl. Five serial (10x) dilutions (10x, 10^2x, 10^3x, 10^4x, 10^5x) of the resulting solution of bacteria, NP and NaCl 0.85% were used to reduce the amount of Colony Forming Units to a number that is easier to count (Figure 15).

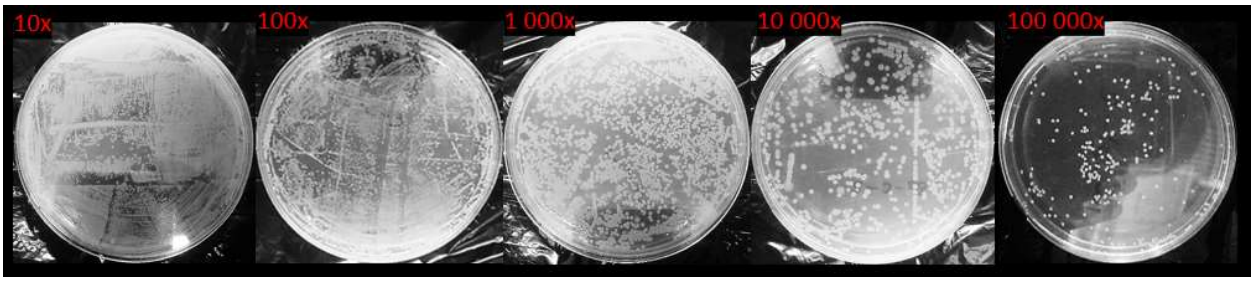

Figure 15.- Example of Agar Plates. Photos correspond to the control, which is E. coli bacteria in broth. Dilutions are made in NaCl. From left to right: Tubes 1 (10x dilution) through 5 (10^5x dilution). Tube 1 has higher concentration of bacteria, more CFU and are difficult to count compared to Tube 5, which is more diluted.

The less diluted (10x to 10^3x) had very high values of CFU (colony forming units), and as such were considered too numerous to count (TNTC). The optimal amount of CFU (30-300 units, allowing for the most accurate count) was achieved for most formulations at 10^4x dilution. A 10^5x dilution was also performed but resulted in all of the formulations having 0 CFU (too few to count: TFTC). Therefore, results are presented for the 10^4x dilution only.

Tests were initally performed in the absence of the PEI modified Ag NP formulations. For a second round of Agar Plate tests that were performed at a later date, similar dilutions were used as for the initial formulations. The use of a 5 min test for PEI also resulted in a 100% reduction.

Table 8.- Average reductions observed after a 10^4x dilution in NaCl 0.85% of the resulting solution from 1 min of exposure of the E. coli bacteria to the Ag NP. Reductions and standard deviations are determined from triplicate samples. Bar graphs of these results and detailed experiment results are presented in Appendix A.5.

Coating	Reduction %
N. Control	0 ± 0
P. Control	100 ± 0
citrate-Ag NPs	92 ± 1
1.5 mg/mL PVP-Ag NPs	100 ± 1
3 mg/mL PVP-Ag NPs	90 ± 1
4.5 mg/mL PVP-Ag NPs	87 ± 1
1.5 mg/mL PEG-Ag NPs	99 ± 1
3 mg/mL PEG-Ag NPs	89 ± 1

Coating	Reduction %
4.5 mg/mL PEG-Ag NPs	92 ± 1
1 µg/mL chitosan-Ag NPs	99 ± 1
3 µg/mL chitosan -Ag NPs	91 ± 1
5 µg/mL chitosan -Ag NPs	94 ± 1
1.5 mg/mL PEI-Ag NPs	94 ± 2
3 mg/mL PEI-Ag NPs	94 ± 2
4.5 mg/mL PEI-Ag NPs	95 ± 2

As we can see from these results, all of the NPs had a very high bactericidal activity (Table 8), even for the short 1 min exposures to the Ag NP. Another experiment was performed using a 5 min exposure of all formulations and the 10^3x, 10^4x and 10^5x dilutions. The results of these experiments were 0 CFU, corroborating the high bactericidal properties of the NP formulations.

The cellular membrane in most bacteria provides the organisms with a negative charge. When they are exposed to the negatively charged nanoparticles, an electrostatic repulsion is expected to limit the cell-particle interactions. In contrast, positively charged nanoparticles would be attracted to the cells, inducing a higher degree of interaction. In the literature, the higher toxicity of positively charged AgNPs is usually attributed to this phenomena[14]. Nonetheless, our results showed no clear trend among the different coatings. Interestingly, with the exception of the PEI,

higher efficacities (i.e. 99% or 100% reductions) were generally observed for the formulations with the least amount of coating.

The most likely explanation for these results is related to the small sizes of the nanoparticles, which are around 10-12 nm. Nanoparticles this small are generally reported to have a very high toxicity[8] and antibacterial efficacy[54]. As a consequence, all of our formulations showed nearly 100% reduction, meaning that is was difficult to see a clear trend.

3.5 MIC (Minimum Inhibitory Concentration)

Minimum Inhibitory Concentrations can also be measured to assess the bactericidal capacities of nanoparticles. In this test, 20 µL of bacteria is added to progressive dilutions of the NPs. The bacteria are exposed to NPs for 24 hours. Larger dilutions (i.e. lower Ag NP concentrations) show a clearer solution (less turbid) than smaller dilutions (Figure 16). The milkiness (turbidity) present in the solution indicates that the bacteria were able to grow. The most diluted NP solutions (with lowest NP concentrations) resulted in the lowest turbidity, thus lowest bactericidal growth. The minimum concentration of NP that prevents visible growth is then taken to be the MIC.

Figure 16.- MIC experiment of E. coli, performed in TSB Broth with 20 µL of bacteria and decreasing concentrations of the Ag NPs. Note the presence of white precipitates in the cells.

When using TSB Broth as the culture medium, MIC measurements showed precipitates at high Ag NP concentrations. At lower concentrations, no milkness or turbidity was observed that would indicate bacterial formation. This observation suggested that growth inhibition was achieved at very low concentrations. So far, in all of the experiments, TSB was the broth of choice. However, in order to rule out the effect of precipitation, the MIC test was performed again (Figure 17), this time using BHI broth as the control and as the medium used to dilute the NPs and grow the bacteria.

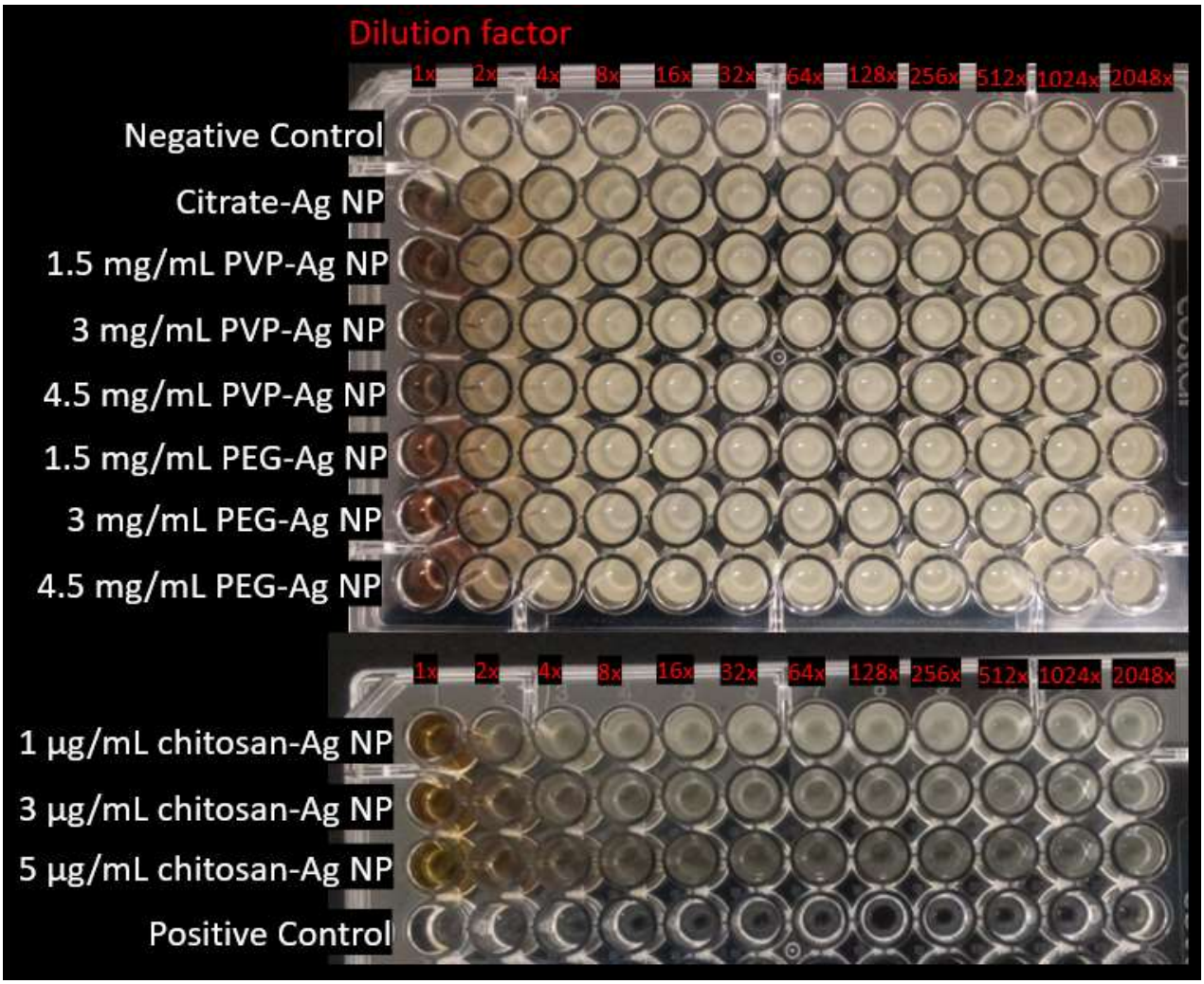

Figure 17.- MIC experiment of E. coli, performed in BHI culture medium and decreasing concentrations of the Ag NPs formulations. Contrasted with Figure 16, there is far less evidence of precipitation. Beside every figure we can find labels showing which coating has the Ag NPs in each row.

Results obtained in the BHI weren't definitive either. As seen in the figure, there were no discernible differences between the nature of the control wells and those of the NPs. The red-brown color that was observed at higher concentrations is the regular color of the Ag NPs, which disappeared when diluted in broth.

3.6 MBC (Minimum Bactericidal Concentration)

In spite of the fact that the MIC results were not conclusive, it was possible to extrapolate a Minimum Bactericidal Concentration from these experiments. Aliquots from the MIC wells were spread over Agar Plates to measure the MBC using BHI broth in order to avoid issues with precipitation.

Table 9.- MBC results using aliquots from previous MIC wells and spreading over Agar Plates. Minimum Bactericidal Concentration is taken as the minimum dilution of Ag NP stock solution that didn't show any bacterial growth. The results are paired with the original concentration of the NPs and were used to calculate the real MBC.

NP formulation	Original NP Concentration (mg Ag/L)	Dilution of the NP stock solution	Minimum Bactericidal Concentration (ng Ag/L)
citrate-Ag NPs	30.3	256x	118
1.5 mg/mL PVP-Ag NPs	37.6	256x	146
3 mg/mL PVP-Ag NPs	43.9	512x	86
4.5 mg/mL PVP-Ag NPs	39.8	256x	155
1.5 mg/mL PEG-Ag NPs	38.2	256x	149
3 mg/mL PEG-Ag NPs	40.1	256x	78
4.5 mg/mL PEG-Ag NPs	39.3	256x	153
1 µg/mL chitosan-Ag NPs	48.7	512x	95
3 µg/mL chitosan-Ag NPs	47.5	512x	93
5 µg/mL chitosan-Ag NPs	40.6	256x	158

MBC test results show that all of the formulations had a very low minimum bactericidal concentration. The first colonies were seen around 256x dilution and in some cases 512x. Using the results from acid digestions to obtain the original concentration of the NPs, we can calculate the MBC as a concentration value (Table 9). The results are in the range of 80 ng/L to 160 ng/L, and there is no clear trend that sets apart one coating from another. In fact, the formulations with the greatest amounts of coating proved to be the closest in value.

3.7 Biofilms

The formulations with the highest concentration of coating were chosen to perform experiments with bacterial biofilms. The selection was made taking in consideration the charges of the formulations, given that 4.5 mg/mL PEI-Ag NPs was the most positive NP, 4.5 mg/mL PEG-Ag NPs was the most negative one and 4.5 mg/mL PVP-Ag NPs was the closest to neutral. The citrate-Ag NPs and the 5 mg/mL chitosan-Ag NPs were also included in the test. Images taken through the confocal microscope were separated in two channels: green (living bacteria) and red (dead bacteria) using the dyes (Figure 18).

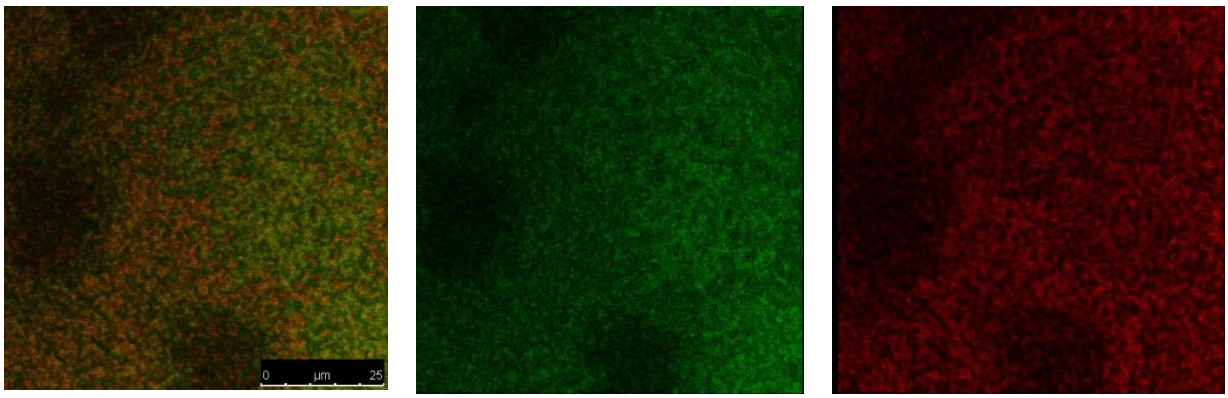

Figure 18.- Biofilm images seen through confocal microscope after 5 min exposure to Ag NPs. Left: combined channels Center: green channel (living bacteria) Right: red channel (dead bacteria)

As a general trend, Table 10 and Table 11 and show that 5 min exposures resulted in higher percentages of dead cells than did the 1 min exposures. For 1 min exposures all of the

formulations had relatively close bactericidal values, which were not too different from the negative control, meaning that they all had low anti-biofilm activity. Reduction percents in the agar plate experiments (Section 3.4) for these experiments were close to 100%, the same as the positive control used (ethanol). In comparison, after allowing the bacteria to form biofilms, the percentage of dead cells (and the reduction percent compared to the positive control) of our formulations are low, suggesting that the biofilms protect the bacteria against potential bactericidal agents.

Table 10.- Confocal microscope results showing anti-biofilm activity of Ag NP formulations. Percentage of dead cells after E. coli has been exposed for 1 min to Ag NP solutions. Five replications were made. Graphs are found in Appendix A.6 (Figure A28).

Coating	Percentage of dead cells	Std Error (N=5)	Reduction %
citrate-Ag NPs	20.7	0.3	9
4.5 mg/mL PVP-Ag NPs	22.7	2.0	17
4.5 mg/mL PEG-Ag NPs	22.9	1.2	17
5 mg/mL chitosan-Ag NPs	23.5	0.6	20
4.5 mg/mL PEI-Ag NPs	21.5	1.2	12
Negative Control (No NPs)	18.7	0.9	0
Positive Control (Ethanol)	42.9	2.5	100

Table 11.- Confocal microscope results showing the anti-biofilm activity of Ag NP formulations. Percentage of dead cells after E. coli bacteria has been exposed for 5 min to Ag NPs solutions. Five replications were made. Graphs in Appendix A.6 (Figure A28).

Coating	Percentage of dead cells	Std Error (N=5)	Reduction %
citrate-Ag NPs	30.3	1.6	40
4.5 mg/mL PVP-Ag NPs	25.1	1.7	22
4.5 mg/mL PEG-Ag NPs	34.8	1.1	56
5 mg/mL chitosan-Ag NPs	29.6	1.9	38

4.5 mg/mL PEI-Ag NPs	24.9	1.1	22
Negative Control	18.6	1.0	0
Positive Control	47.7	3.8	100

For the 5 min exposures, the percentage of dead cells increased for all formulations. The percent reduction allowed us to see that the increase was fairly considerable for these formulations that had more time to penetrate the biofilm. We can also see that the negatively coated nanoparticles, including the chitosan modified formulations gave better results than the rest. PVP (slightly negative) and PEI (slightly positive) modified NPs gave a similar percentage of dead cells.

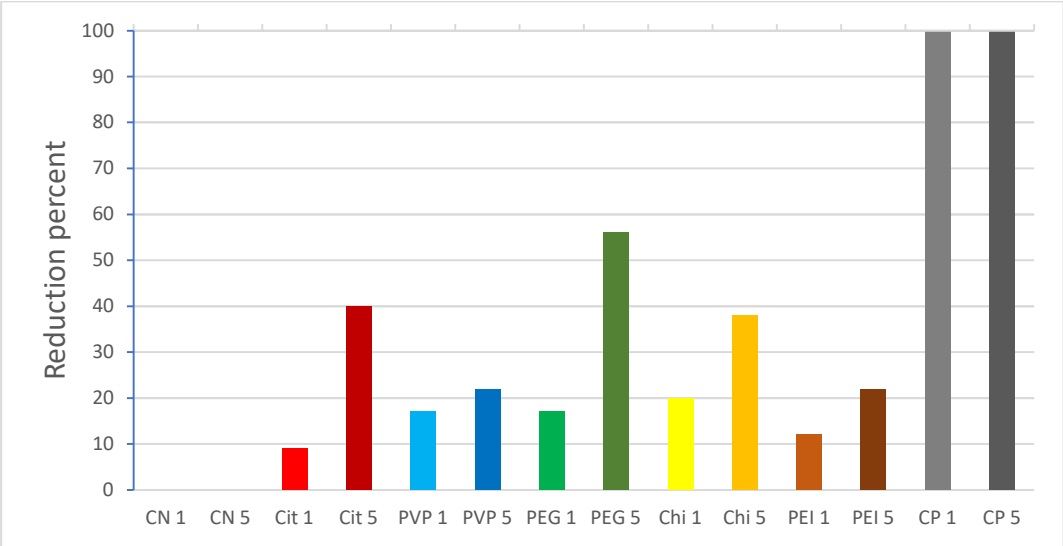

Figure 19.- Confocal microscope results showing anti-biofilm activity of Ag NP formulations. To better compare results of the two exposure times, reduction percents compared to the positive control were calculated. Negative control was taken as the minimum, positive control was taken as the maximum.

Given that all formulations had very similar antibacterial activities determined by MIC and Agar Plate experiments, the differences of anti-biofilm activities that were observed suggest that they play an important role in bacterial resistance. The results suggested that the negative coatings confered higher antibiofilm activity to the nanoparticles, compared to those with a positive charge or a small negative charge.

A study of layer by layer coated nanoparticles has shown that nanoparticles performed worse when interacting with *E. coli* biofilms when the external layer was positively charged than when it was negatively charged[70]. It is suggested that interactions between positively charged polymers and biofilms can lead to cell aggregation and bacterial sedimentation on the surfaces. Electrostatic interactions between the positive polymers and the negative cells can induce biofilm formation. The cells aggregate and form clusters where bacteria are grown and the polymers bind to the outer cell membrane and agglomerate *E. coli* cells into the biofilms clusters on the surface[71]. Positively charged surfaces favoring biofilm formation, which lead to further protection for bacteria, could be a possible explanation for the PEI coated formulations that performed worse than the negatively charged nanoparticles.

Chapter 4 – Conclusions

Silver nanoparticles have proven to have antibacterial effects and could represent an alternative to antibiotics in medical treatments against multi drug resistant bacteria. The study of their physicochemical properties could lead to more effective usage of these Ag NPs and reduce the potential harmful effect on the environment if they are overused. For this study, several formulations of Ag NPs were synthesized and stabilized with citrate, then coated with polymers, and was evaluated how the zeta potential of the nanoparticles was affected with the addition of coating.

Coatings were selected based on the surface charge modification reported in literature: PEG (negative), PVP (neutral) and chitosan (positive). After characterization with SP-ICPMS, it was determined that Ag NPs were similar in concentration and size (around 5 nm of radius) while hydrodynamic radius measured by DLS varied with the addition of coating, showing a range between 13 and 26 nm of radii. Zeta potential measurements showed that PEG coated Ag NPs had a high negative value (-38 mV to -46 mV); while PVP coated were slightly negative (-7 mV to -15 mV), presumably due to adsorption of excess anions during synthesis into the coated surface of the nanoparticles, that were unable to be removed after centrifugation and washing. Citrate stabilized NPs had also a negative zeta potential (-24 mV). However, chitosan coated NPs failed to achieve a positive charge as intended. Another positive charge modifying coating, like PEI was introduced later in the study. Zeta potential measurements of these PEI formulations resulted in moderately positive values (9 mV to 16 mV) and deagglomerated after adjusting the pH close to 7.

E. coli bacteria was used as the target of experiments using the Ag NPs formulations. Percent reduction was high for all formulations and no clear trend was obtained. Similarly, the MBC was very low for all formulations suggesting that they had very effective biocidal properties regardless of surface charge or coating. It must be noted that NPs this small are widely regarded as very toxic for bacteria, effectively killing most of the bacteria in agar plate experiments (90 % to 100 % reduction in all cases after 1 min exposure, 100% in all cases after 5 min exposure) and making

unable to differentiate if some coatings were enhancing the antibacterial effect more than others.

When Ag NP formulations were applied to biofilm protected *E. coli* the percentage of dead cells (obtained through confocal microscopy) were much lower than at contact with ethanol, used as positive control. This contrasts with the results against bacteria with no biofilm, suggesting that the biofilm manages to lower the biocidal effects of the nanoparticles. Moreover, we can see that PEG-Ag NPs had the highest anti biofilm effect while PVP-Ag NPs and PEI-Ag NPs had the lowest. Being that the NPs are close in concentration, size, antibacterial effect and were even synthesized in the same conditions, this indicates that negative charge modifying coatings grant greater antibiofilm effects compared to neutral or positive ones. Still, it must be taken in account that PEI coated NPs had lower absolute charge value than PEG coated ones, meaning their stability is lower. While nanoparticles with a positively charged surface are generally considered to have higher antibacterial activity, our results suggest that when used against *E. coli* biofilms they perform worse than Ag NPs with a negative surface charge.

More research is required, with Ag NPs with higher positive zeta potential, to evaluate if anti biofilm activity would be enhanced or hindered with the increase in surface charge. It would also be useful to have more coatings tested, to check what would be the effect of different coatings that result in similar charge. PEI coated formulations required more characterization, as they weren't part of the study until late and analysis such as SP-ICPMS and MIC weren't performed in time. Our results from chitosan and PEG (both with ζ near -40 mV) suggest that the coating molecule could be also playing a factor, but results aren't definitive as chitosan formulation had very low coating concentration and its charge is not attributed to the coating itself. Other bacterial strains could be used in future experiments to see if they are affected the same way as *E. coli*. Lastly, FCS experiments to study the diffusion of Ag NPs through biofilm were not completed but are planned as a continuation of this research.

Bibliographic References

1. Bassetti, M.; Righi, E., Multidrug-resistant bacteria: what is the threat? *American Society of Hematology* **2013,** *2013*, (1), 428-432.
2. van Duin, D.; Paterson, D. L., Multidrug-Resistant Bacteria in the Community: Trends and Lessons Learned. *Infectious Disease Clinics of North America* **2016,** *30*, (2), 377-390.
3. Seil, J. T.; Webster, T. J., Antimicrobial applications of nanotechnology: methods and literature. *International Journal of Nanomedicine* **2012,** *7*, 2767-2781.
4. Franci, G.; Falanga, A.; Galdiero, S.; Palomba, L.; Rai, M.; Morelli, G.; Galdiero, M., Silver nanoparticles as potential antibacterial agents. *Molecules* **2015,** *20*, (5), 8856-8874.
5. Singh, M.; Singh, S.; Prasad, S.; Gambhir, I. S., Nanotechnology in medicine and antibacterial effect of silver nanoparticles. *Digest Journal of Nanomaterials and Biostructures* **2008,** *3*, (3), 115-122.
6. Marambio-Jones, C.; Hoek, E. M. V., A review of the antibacterial effects of silver nanomaterials and potential implications for human health and the environment. *Journal of Nanoparticle Research* **2010,** *12*, (5), 1531-1551.
7. Dos Santos, C. A.; Seckler, M. M.; Ingle, A. P.; Gupta, I.; Galdiero, S.; Galdiero, M.; Gade, A.; Rai, M., Silver nanoparticles: therapeutical uses, toxicity, and safety issues. *Journal of Pharmaceutical Sciences* **2014,** *103*, (7), 1931-1944.
8. Ivask, A.; Kurvet, I.; Kasemets, K.; Blinova, I.; Aruoja, V.; Suppi, S.; Vija, H.; Kakinen, A.; Titma, T.; Heinlaan, M.; Visnapuu, M.; Koller, D.; Kisand, V.; Kahru, A., Size-dependent toxicity of silver nanoparticles to bacteria, yeast, algae, crustaceans and mammalian cells in vitro. *PLoS One* **2014,** *9*, (7), e102108.
9. Jain, J.; Arora, S.; Rajwade, J. M.; Omray, P.; Khandelwal, S.; Paknikar, K. M., Silver Nanoparticles in Therapeutics: Development of an Antimicrobial Gel Formulation for Topical Use. *Molecular Pharmaceutics* **2009,** *6*, (5), 1388-1401.
10. Le Ouay, B.; Stellacci, F., Antibacterial activity of silver nanoparticles: A surface science insight. *Nano Today* **2015,** *10*, (3), 339-354.
11. Morones, J. R.; Elechiguerra, J. L.; Camacho, A.; Holt, K.; Kouri, J. B.; Ramirez, J. T.; Yacaman, M. J., The bactericidal effect of silver nanoparticles. *Nanotechnology* **2005,** *16*, (10), 2346-2353.
12. Gontijo, L. A. P.; Raphael, E.; Ferrari, D. P. S. F. J. L.; Lyon, J. P.; Schiavon, M. A., pH effect on the synthesis of different size silver nanoparticles evaluated by DLS and their size-dependent antimicrobial activity. *revista Materia* **2020,** *25*, (04), 1-9.
13. Jo, D. H.; Kim, J. H.; Lee, T. G.; Kim, J. H., Size, surface charge, and shape determine therapeutic effects of nanoparticles on brain and retinal diseases. *Nanomedicine* **2015,** *11*, (7), 1603-1611.
14. Badawy, A. M. E.; Silva, R. G.; Morris, B.; Scheckel, K. G.; Suidan, M. T.; Tolaymat, T. M., Surface Charge-Dependent Toxicity of Silver Nanoparticles. *Environmental Science & Technology* **2011,** *45*, 283-287.
15. Duan, X.; Li, Y., Physicochemical characteristics of nanoparticles affect circulation, biodistribution, cellular internalization, and trafficking. *Small* **2013,** *9*, (9-10), 1521-1532.
16. Murray, P. R.; Rosenthal, K. S.; Pfaller, M. A., *Medical microbiology E-book*. Elsevier Health Sciences: 2020.
17. Slonczewski, J. F. J. W., *Microbiology : an evolving science*. W.W. Norton & Co.: New York, 2009.
18. Shih, Y. L.; Rothfield, L., The bacterial cytoskeleton. *Microbiology & Molecular Biology Reviews* **2006,** *70*, (3), 729-754.

19. Pommerville, J. C. P. J. C., *Fundamentals of microbiology*. Jones & Bartlett Learning: Burlington, MA, 2014.
20. Thanbichler, M.; Wang, S. C.; Shapiro, L., The bacterial nucleoid: a highly organized and dynamic structure. *Journal of Cellular Biochemistry* **2005,** *96*, (3), 506-521.
21. Jeong, S. W.; Choi, Y. J., Extremophilic Microorganisms for the Treatment of Toxic Pollutants in the Environment. *Molecules* **2020,** *25*, (21), 1-16.
22. Krasner, R. I. S. T., *The microbial challenge : a public health perspective*. Jones & Bartlett Learning: Burlington, Mass., 2013.
23. Wheelis, M., *Principles of modern microbiology*. Jones and Bartlett Publishers: Sudbury, Mass. ;, 2008.
24. Walsh, F. M.; Amyes, S. G., Microbiology and drug resistance mechanisms of fully resistant pathogens. *Current Opinion in Microbiology* **2004,** *7*, (5), 439-444.
25. Denamur, E.; Matic, I., Evolution of mutation rates in bacteria. *Molecular Microbiology* **2006,** *60*, (4), 820-827.
26. Davey, M. E.; O'Toole, G. A., Microbial Biofilms: from Ecology to Molecular Genetics. *Microbiology and Molecular Biology Reviews* **2000,** *64*, (4), 847-867.
27. Donlan, R. M.; Costerton, J. W., Biofilms: survival mechanisms of clinically relevant microorganisms. *Clinical Microbiology Reviews* **2002,** *15*, (2), 167-193.
28. Karatan, E.; Watnick, P., Signals, regulatory networks, and materials that build and break bacterial biofilms. *Microbiology and Molecular Biology Reviews* **2009,** *73*, (2), 310-347.
29. Patel, C. N.; Wortham, B. W.; Lines, J. L.; Fetherston, J. D.; Perry, R. D.; Oliveira, M. A., Polyamines are essential for the formation of plague biofilm. *Journal of Bacteriology* **2006,** *188*, (7), 2355-2363.
30. Klasen, H. J., A historical review of the use of silver in the treatment of burns. II. Renewed interest for silver. *Burns* **2000,** *26*, 131-138.
31. Ahmad, A.; Mukherjee, P.; Senapati, S.; Mandal, D.; Khan, M. I.; Kumar, R.; Sastry, M., Extracellular biosynthesis of silver nanoparticles using the fungus Fusarium oxysporum. *Colloids and Surfaces B: Biointerfaces* **2003,** *28*, (4), 313-318.
32. Rai, M.; Kon, K.; Ingle, A.; Duran, N.; Galdiero, S.; Galdiero, M., Broad-spectrum bioactivities of silver nanoparticles: the emerging trends and future prospects. *Applied Microbiology & Biotechnology* **2014,** *98*, (5), 1951-1961.
33. Chowdhury, S.; Basu, A.; Kundu, S., Green synthesis of protein capped silver nanoparticles from phytopathogenic fungus *Macrophomina phaseolina* (Tassi) Goid with antimicrobial properties against multidrug-resistant bacteria. *Nanoscale Research Letters* **2014,** *9*, (365), 1-11.
34. Kalishwaralal, K.; BarathManiKanth, S.; Pandian, S. R.; Deepak, V.; Gurunathan, S., Silver nanoparticles impede the biofilm formation by Pseudomonas aeruginosa and Staphylococcus epidermidis. *Colloids and Surfaces B Biointerfaces* **2010,** *79*, (2), 340-344.
35. AshaRani, P. V.; Mun, G. L. K.; Hande, M. P.; Valiyaveettil, S., Cytotoxicity and Genotoxicity of Silver Nanoparticles in Human Cells. *American Chemical Society Nano* **2009,** *3*, (2), 279-290.
36. Holt, K. B.; Bard, A. J., Interaction of Silver (I) Ions with the Respiratory Chain of Escherichia coli: An Electrochemical and Scanning Electrochemical Microscopy Study of the Antimicrobial Mechanism of Micromolar Ag. *Biochemistry* **2005,** *44*, 13214-13223.
37. Choi, O.; Hu, Z., Size Dependent and Reactive Oxygen Species Related Nanosilver Toxicity to Nitrifying Bacteria. *Environmental Science & Technology* **2008,** *42*, 4583-4588.
38. Sondi, I.; Salopek-Sondi, B., Silver nanoparticles as antimicrobial agent: a case study on E. coli as a model for Gram-negative bacteria. *Journal of Colloid and Interface Science* **2004,** *275*, (1), 177-182.

39. Li, W. R.; Xie, X. B.; Shi, Q. S.; Zeng, H. Y.; Ou-Yang, Y. S.; Chen, Y. B., Antibacterial activity and mechanism of silver nanoparticles on Escherichia coli. *Applied Microbiology & Biotechnology* **2010,** *85*, (4), 1115-1122.
40. Li, X. Z.; Nikaido, H.; Williams, K. E., Silver-resistant mutants of Escherichia coli display active efflux of Ag+ and are deficient in porins. *Journal of Bacteriology* **1997,** *179*, (19), 6127-6132.
41. Buffle, J.; Wilkinson, K. J.; Stoll, S.; Filella, M.; Zhang, J., A Generalized Description of Aquatic Colloidal Interactions: The Three-colloidal Component Approach. *Environmental Science & Technology* **1998,** *32*, 2887-2899.
42. Pate, K.; Safier, P., Chemical metrology methods for CMP quality. In *Advances in Chemical Mechanical Planarization (CMP)*, 2016; pp 299-325.
43. Mayers, D., Electrostatic Forces and the Electrical Double Layer Colloids and Colloidal Stability. *Surfaces, Interfaces, and Colloids* **2002**, 79-96.
44. Russel, W. B.; Saville, D. A.; Schowalter, W. R., *Colloidal Dispersions*. Cambridge University Press: Cambridge, 1989.
45. Hanaor, D. A. H.; Michelazzi, M.; Leonelli, C.; Sorrell, C. C., The Effects of Carboxylic Acids on the Aqueous Dispersion and Electrophoretic Deposition of ZrO_2. *Journal of the European Ceramic Society* **2012,** *32*, (1), 235-244.
46. Foster, K. A.; Yazdanian, M.; Audus, K. L., Microparticulate uptake mechanisms of in-vitro cell culture models of the respiratory epithelium. *Journal of Pharmacy and Pharmacology* **2001,** *53*, 57-66.
47. Bernfield, M.; Götte M Fau - Park, P. W.; Park Pw Fau - Reizes, O.; Reizes O Fau - Fitzgerald, M. L.; Fitzgerald Ml Fau - Lincecum, J.; Lincecum J Fau - Zako, M.; Zako, M., Functions of cell surface heparan sulfate proteoglycans. *Annual Review of Biochemistry* **1999,** *68*, (0066-4154 (Print)), 729-77.
48. Kelf, T. A.; Sreenivasan, V. K. A.; Sun, J.; Kim, E. J.; Goldys, E. M.; Zvyagin, A. V., Non-specific cellular uptake of surface-functionalized quantum dots. *Nanotechnology* **2010,** *21*, (28), 1-14.
49. Patil, S.; Sandberg, A.; Heckert, E.; Self, W.; Seal, S., Protein adsorption and cellular uptake of cerium oxide nanoparticles as a function of zeta potential. *Biomaterials* **2007,** *28*, (31), 4600-4607.
50. Honary, S.; Zahir, F., Effect of Zeta Potential on the Properties of Nano-Drug Delivery Systems - A Review (Part 1). *Tropical Journal of Pharmaceutical Research* **2013,** *12*, (2), 255-264.
51. Laborda, F.; Bolea, E.; Jimenez-Lamana, J., Single particle inductively coupled plasma mass spectrometry: a powerful tool for nanoanalysis. *Analytical Chemistry* **2014,** *86*, (5), 2270-2278.
52. Chu, B., II - LIGHT SCATTERING THEORY. In *Laser Light Scattering (Second Edition)*, Chu, B., Ed. Academic Press: 1991; pp 13-61.
53. Berne, B. J.; Pecora, R., *Dynamic light scattering, with application to chemistry, biology and physics*. John Wiley & Sons: 1976; p 376.
54. Agnihotri, S.; Mukherji, S.; Mukherji, S., Size-controlled silver nanoparticles synthesized over the range 5–100 nm using the same protocol and their antibacterial efficacy. *Royal Society of Chemistry Advances* **2014,** *4*, (8), 3974-3983.
55. Korshed, P.; Li, L.; Liu, Z.; Mironov, A.; Wang, T., Size-dependent antibacterial activity for laser-generated silver nanoparticles. *Journal of Interdisciplinary Nanomedicine* **2019,** *4*, (1), 24-33.
56. Bhattarai, N.; Khanal, S.; Pudasaini, P. R.; Pahl, S.; Romero-Urbina, D., Citrate Stabilized Silver Nanoparticles. *International Journal of Nanotechnology and Molecular Computation* **2011,** *3*, (3), 15-28.
57. Jurasin, D. D.; Curlin, M.; Capjak, I.; Crnkovic, T.; Lovric, M.; Babic, M.; Horak, D.; Vinkovic Vrcek, I.; Gajovic, S., Surface coating affects behavior of metallic nanoparticles in a biological environment. *Beilstein Journal of Nanotechnology* **2016,** *7*, 246-262.
58. Pang, C.; Zhang, P.; Mu, Y.; Ren, J.; Zhao, B., Transformation and Cytotoxicity of Surface-Modified Silver Nanoparticles Undergoing Long-Term Aging. *Nanomaterials (Basel)* **2020,** *10*, (11), 1-11.

59. Sharonova, A.; Loza, K.; Surmeneva, M.; Surmenev, R.; Prymak, O.; Epple, M., Synthesis of positively and negatively charged silver nanoparticles and their deposition on the surface of titanium. *IOP Conference Series: Materials Science and Engineering* **2016,** *116*, 1-8.
60. Cinteza, L. O.; Scomoroscenco, C.; Voicu, S. N.; Nistor, C. L.; Nitu, S. G.; Trica, B.; Jecu, M. L.; Petcu, C., Chitosan-Stabilized Ag Nanoparticles with Superior Biocompatibility and Their Synergistic Antibacterial Effect in Mixtures with Essential Oils. *Nanomaterials (Basel)* **2018,** *8*, (10), 1-16.
61. Belteky, P.; Ronavari, A.; Igaz, N.; Szerencses, B.; Toth, I. Y.; Pfeiffer, I.; Kiricsi, M.; Konya, Z., Silver nanoparticles: aggregation behavior in biorelevant conditions and its impact on biological activity. *International Journal of Nanomedicine* **2019,** *14*, 667-687.
62. Mohanta, Y. K.; Biswas, K.; Jena, S. K.; Hashem, A.; Abd Allah, E. F.; Mohanta, T. K., Anti-biofilm and Antibacterial Activities of Silver Nanoparticles Synthesized by the Reducing Activity of Phytoconstituents Present in the Indian Medicinal Plants. *Frontiers in Microbiology* **2020,** *11*, 1143.
63. Miskovska, A.; Rabochova, M.; Michailidu, J.; Masak, J.; Cejkova, A.; Lorincik, J.; Matatkova, O., Antibiofilm activity of silver nanoparticles biosynthesized using viticultural waste. *PLoS One* **2022,** *17*, (8), e0272844.
64. Bruna, T.; Maldonado-Bravo, F.; Jara, P.; Caro, N., Silver Nanoparticles and Their Antibacterial Applications. *International Journal of Molecular Science* **2021,** *22*, (13).
65. Dadosh, T., Synthesis of uniform silver nanoparticles with a controllable size. *Materials Letters* **2009,** *63*, (26), 2236-2238.
66. Tejamaya, M.; Römer, I.; Merrifield, R. C.; Lead, J. R., Stability of citrate, PVP, and PEG coated silver nanoparticles in ecotoxicology media. *Environmental Science & Technology* **2012,** *46*, (13), 7011-7017.
67. Li, X.; Lenhart, J. J., Aggregation and dissolution of silver nanoparticles in natural surface water. *Environmental Science & Technology* **2012,** *46*, (10), 5378-5386.
68. Dickhaus, B. N.; Priefer, R., Determination of polyelectrolyte pKa values using surface-to-air tension measurements. *Colloids and Surfaces A: Physicochemical and Engineering Aspects* **2016,** *488*, 15-19.
69. Gallops, C. E.; Yu, C.; Ziebarth, J. D.; Wang, Y., Effect of the Protonation Level and Ionic Strength on the Structure of Linear Polyethyleneimine. *ACS Omega* **2019,** *4*, (4), 7255-7264.
70. Ivanova, A.; Ivanova, K.; Hoyo, J.; Heinze, T.; Sanchez-Gomez, S.; Tzanov, T., Layer-By-Layer Decorated Nanoparticles with Tunable Antibacterial and Antibiofilm Properties against Both Gram-Positive and Gram-Negative Bacteria. *ACS Applied Materials & Interfaces* **2018,** *10*, (4), 3314-3323.
71. Zhang, P.; Lu, H.; Chen, H.; Zhang, J.; Liu, L.; Lv, F.; Wang, S., Cationic Conjugated Polymers-Induced Quorum Sensing of Bacteria Cells. *Analytical Chemistry* **2016,** *88*, (6), 2985-2988.

Appendix

A.1 Transmission Electron Microscopy

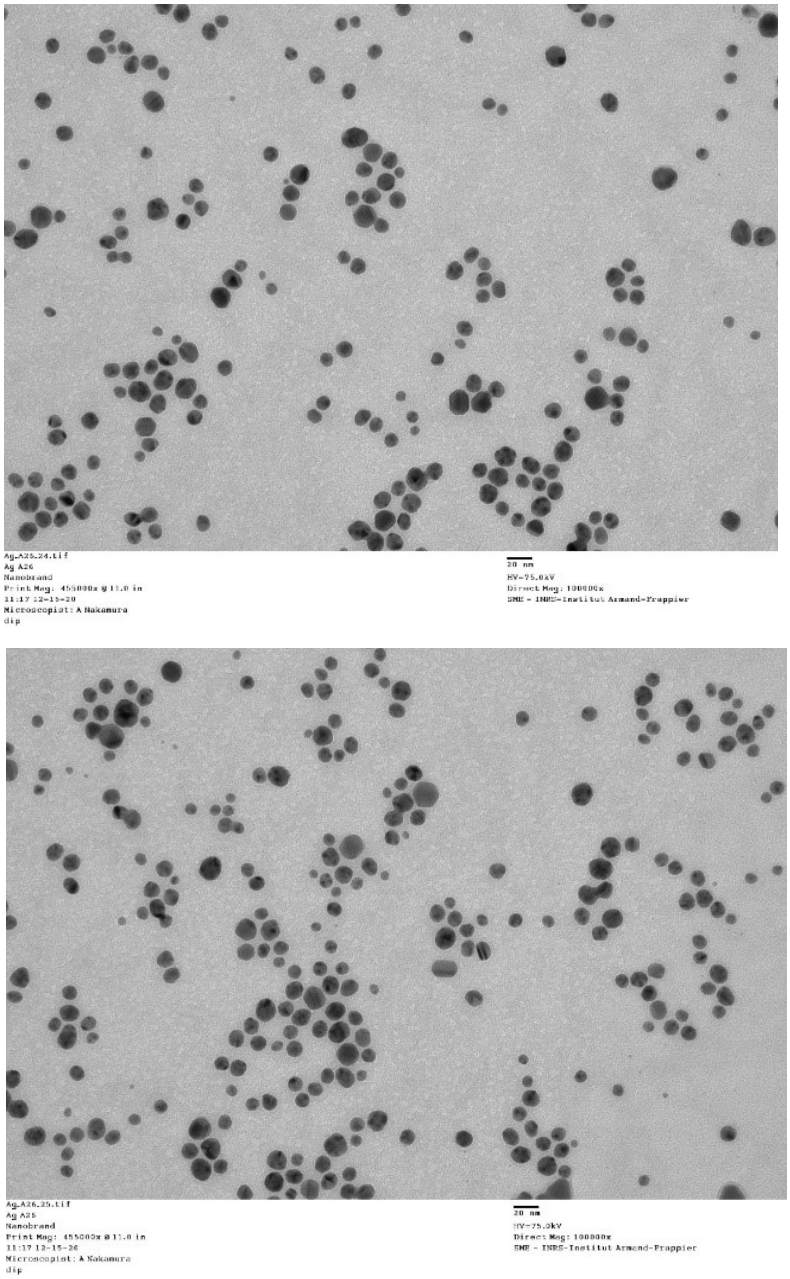

Figure A20.- Images obtained through transmission electron microscopy of the citrate stabilized silver nanoparticles without the addition of coating.

A.2 Size distribution graphs

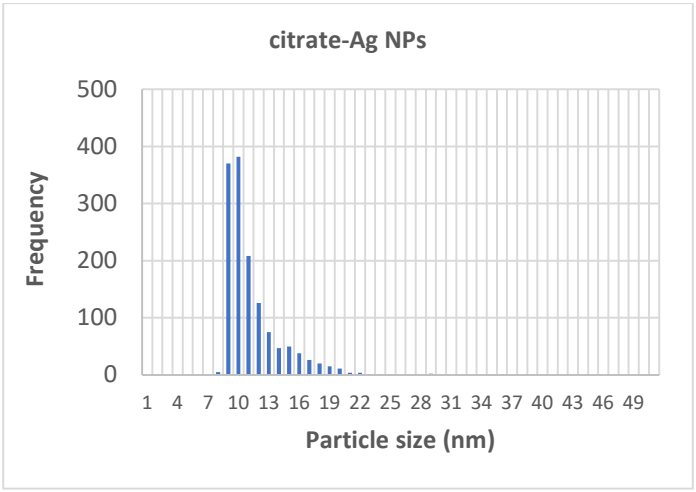

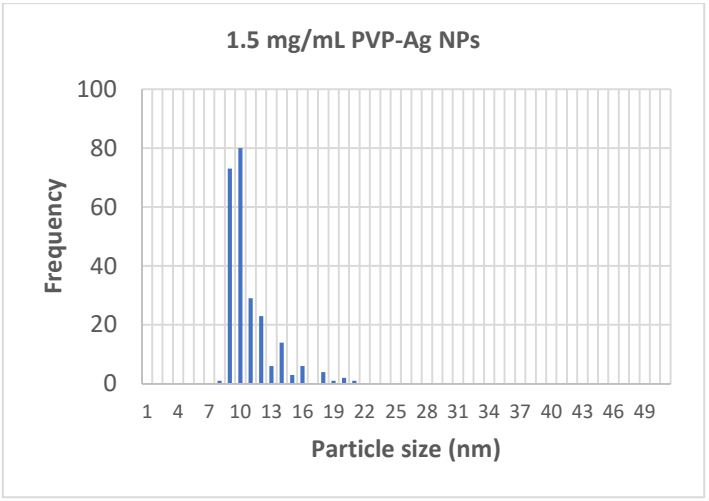

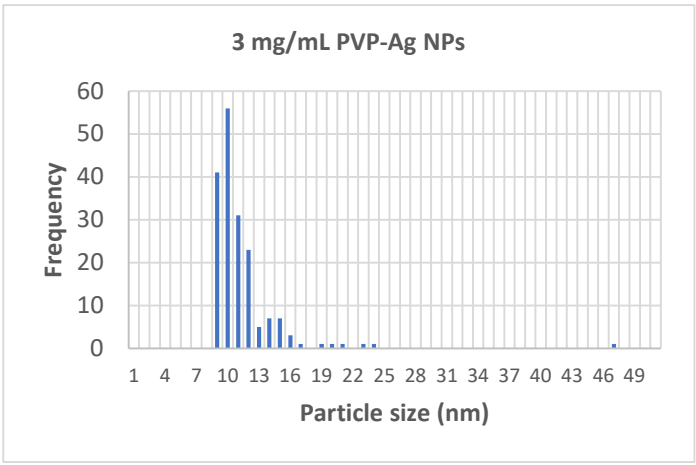

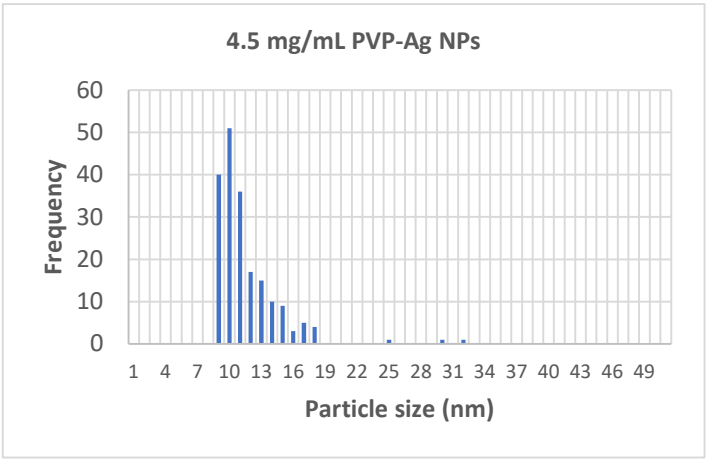

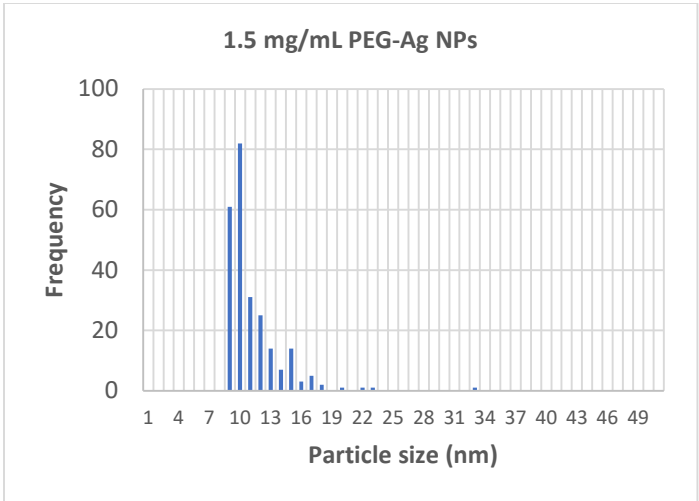

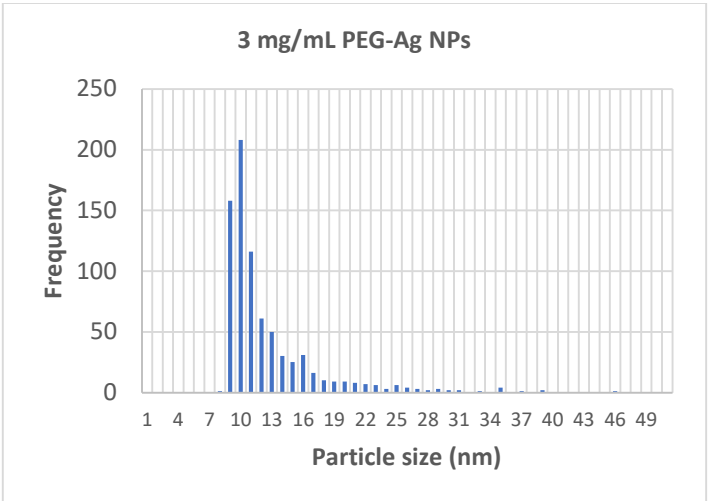

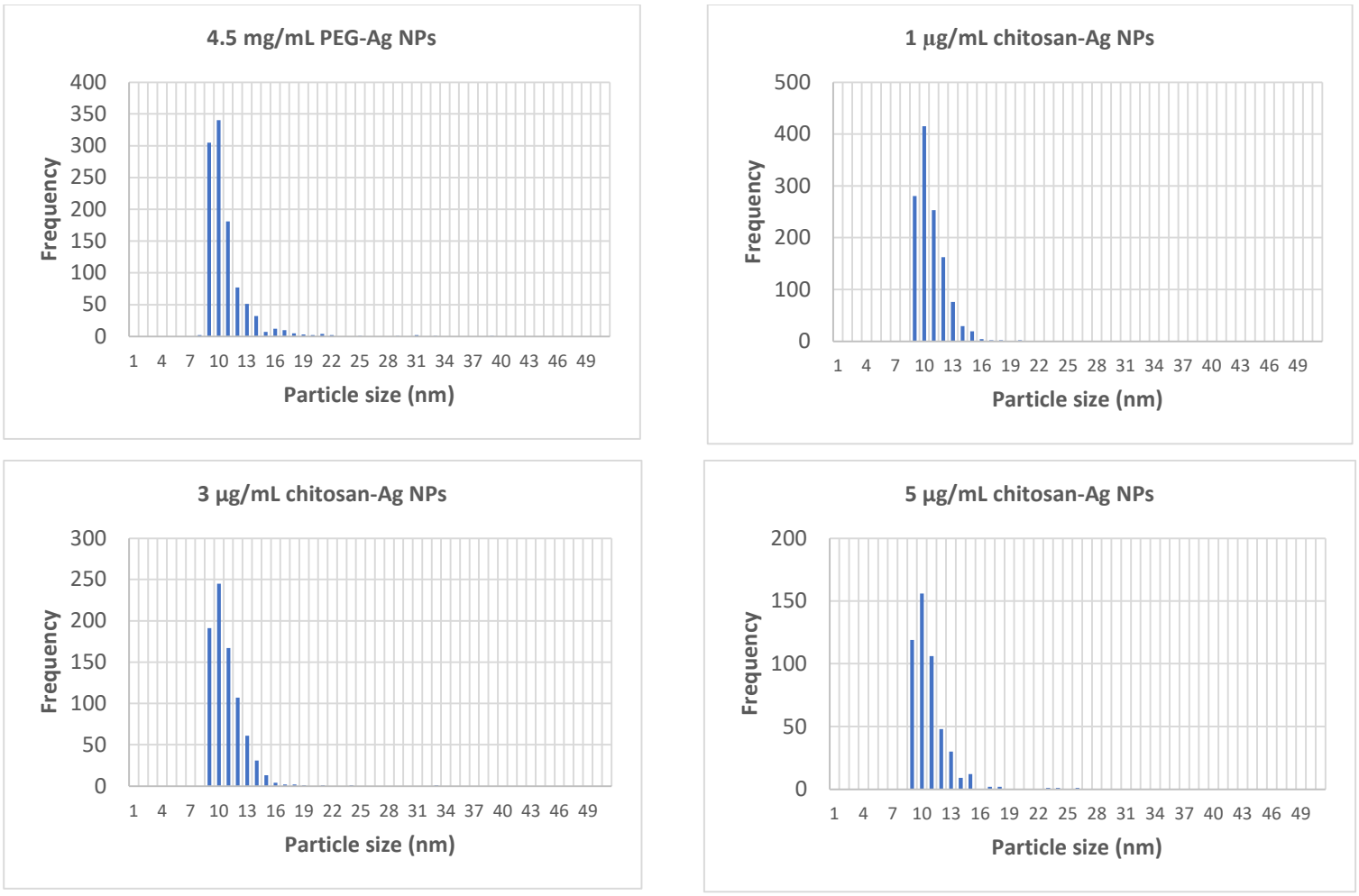

Figure A21.- Particle size distribution of the diameter of the silver nanoparticles as measured by SP-ICPMS. The steep drop off at lower sizes (shark fin shape) suggests that we were close to the size detection limits of the instrument (7 nm).

A.3 Graphs of SP ICPMS results

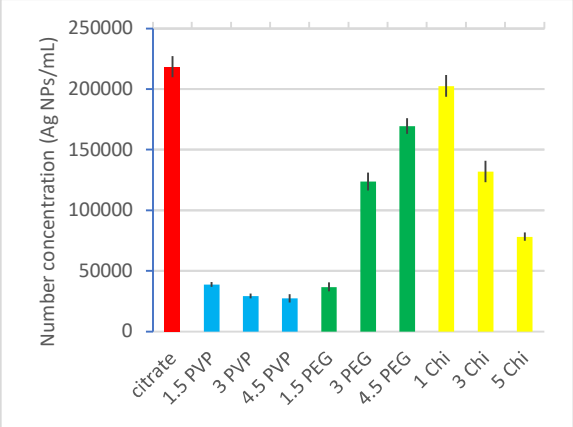

Figure A22. - Comparison of number concentration of Ag NPs. NPs were measured after dilution of the stock solutions by 500 000 times. Formulations are named according to the concentration of the coating in mg/mL (µg/mL in the case of chitosan). Chi refers to chitosan.

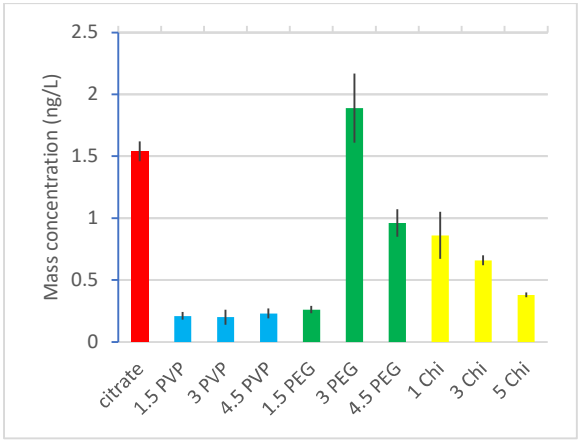

Figure A23.- Comparison of mass concentration of Ag NPs (ng/L). NPs were measured after dilution of the stock solutions by 500 000 times. Formulations are named according to the concentration of the coating in mg/mL (µg/mL in the case of chitosan). Chi refers to chitosan.

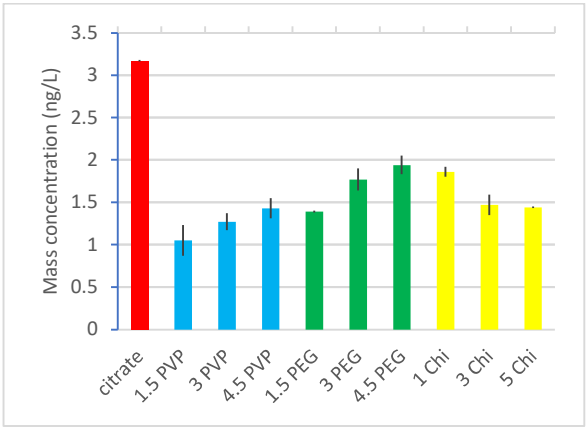

Figure A24.- Comparison of mass concentration of dissolved Ag (ng/L) in Ag NP formulations (no acid digestion). NPs were measured after dilution of the stock solutions by 500 000 times. Formulations are named according to the concentration of the coating in mg/mL (µg/mL in the case of chitosan). Chi refers to chitosan.

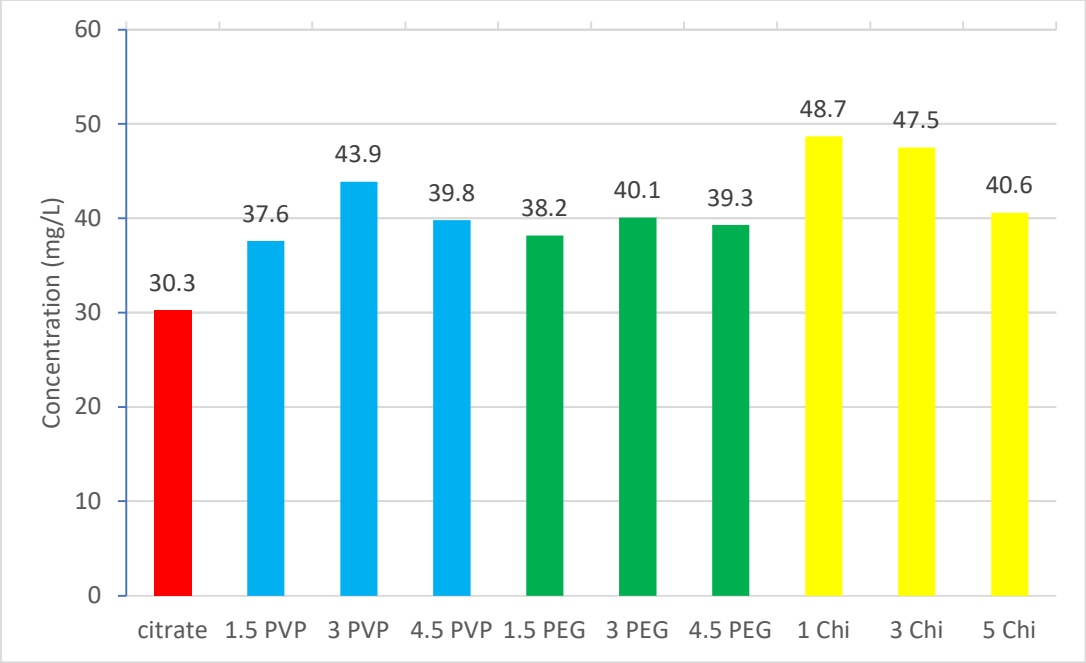

Figure A25.- Total concentration of silver in the AgNP formulations (mg/L) after acid digestion. NPs were measured after dilution of the stock solutions by 500 000 times. Formulations are named according to the concentration of the coating in mg/mL (µg/mL in the case of chitosan). Chi refers to chitosan.

A.4 Zeta potentials graphs

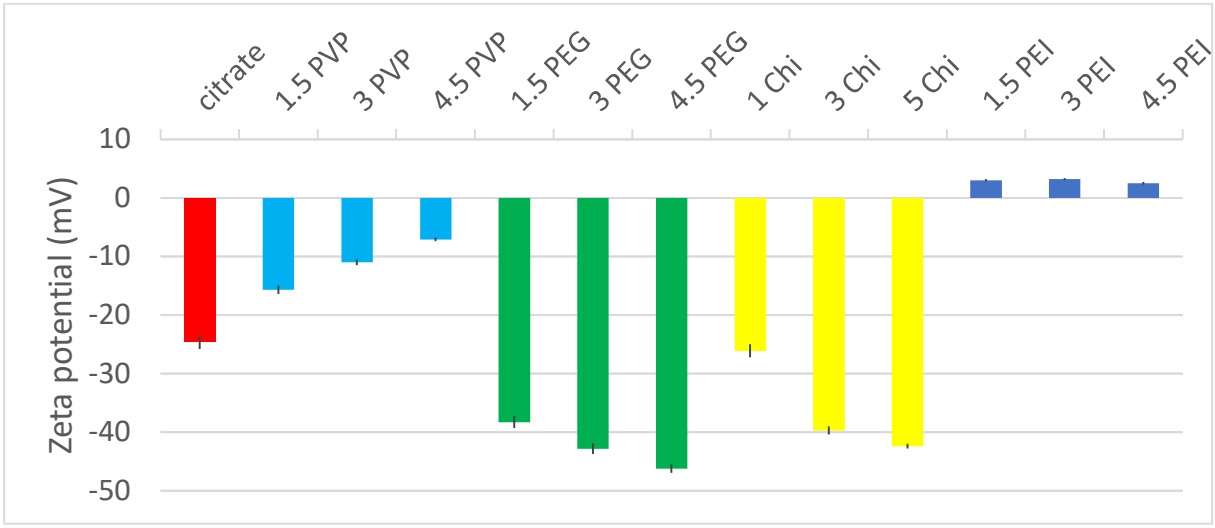

Figure A26.- Initial zeta potentials of Ag NP formulations. Zeta potential was calculated by Smoluchowski Model. Six repetitions of the measurements were performed.

A.5 Agar plate counts

Table A12.- Agar Plate counts of 10^4x dilution results. Ag NP is exposed to the E. coli bacteria for 1 min and then diluted 10^4x in NaCl 0.85%. Reduction % were determined by considering the exposure to the broth only as the negative control (0% reduction).

Coating	CFU	Reduction %	CFU	Reduction %	CFU	Reduction %
Negative Control (Broth)	971	0	683	0	720	0
Positive Control (Ethanol)	0	100	0	100	0	100
citrate-Ag NPs	83	91	41	94	76	89
1.5 mg/mL PVP-Ag NPs	0	100	1	100	0	100
3 mg/mL PVP-Ag NPs	99	90	68	90	66	91
4.5 mg/mL PVP-Ag NPs	106	89	96	86	102	86
1.5 mg/mL PEG-Ag NPs	12	99	0	100	8	99
3 mg/mL PEG-Ag NPs	91	91	75	89	77	89
4.5 mg/mL PEG-Ag NPs	60	94	59	91	66	91
1 µg/mL chitosan-Ag NPs	5	99	2	100	11	98
3 µg/mL chitosan -Ag NPs	94	90	53	92	73	90
5 µg/mL chitosan -Ag NPs	35	96	51	93	48	93

Table A13.- Agar Plate counts of 10^4x results for PEI formulations at a different date, with different Negative Control. As before, E. coli bacteria is exposed to the Ag NP for 1 min and then diluted 10^4x in NaCl 0.85%. Reduction % were determined by considering the exposure to the broth as the negative control (0% reduction).

Coating	CFU	Reduction %	CFU	Reduction %	CFU	Reduction %
Negative Control (Broth)	720	0	669	0	889	0
Positive Control (Ethanol)	0	100	0	100	0	100
1.5 mg/mL PEI-Ag NPs	69	90	25	96	33	96
3 mg/mL PEI-Ag NPs	75	90	29	96	41	95
4.5 mg/mL PEI-Ag NPs	71	90	21	97	17	98

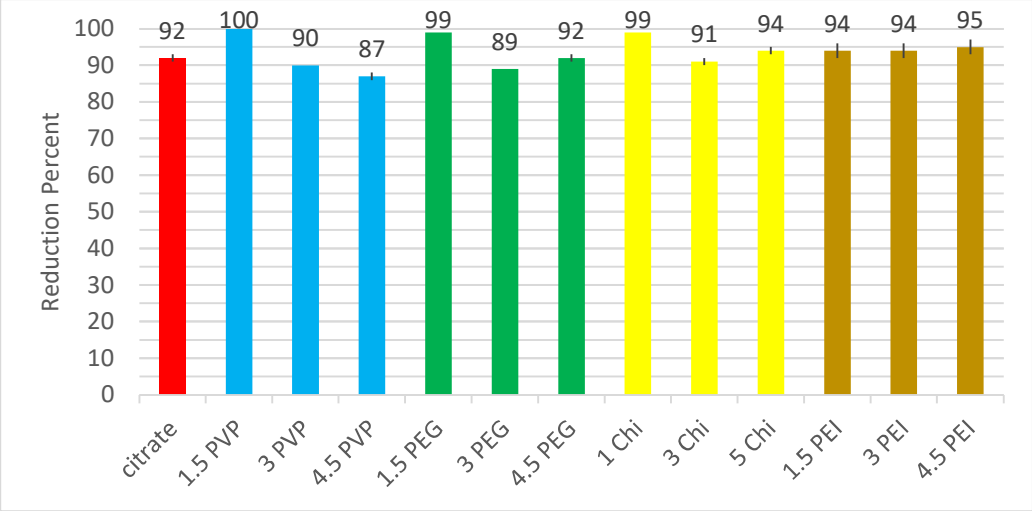

Figure A27.- Comparison of average reductions (N=3) observed after a 10 000x dilution in NaCl of the resulting solution from 1 min of exposure of the E. coli bacteria to the Ag NP. No clear trend of reduction percent with charge is observed.

A.6 Exposure to biofilm graphs

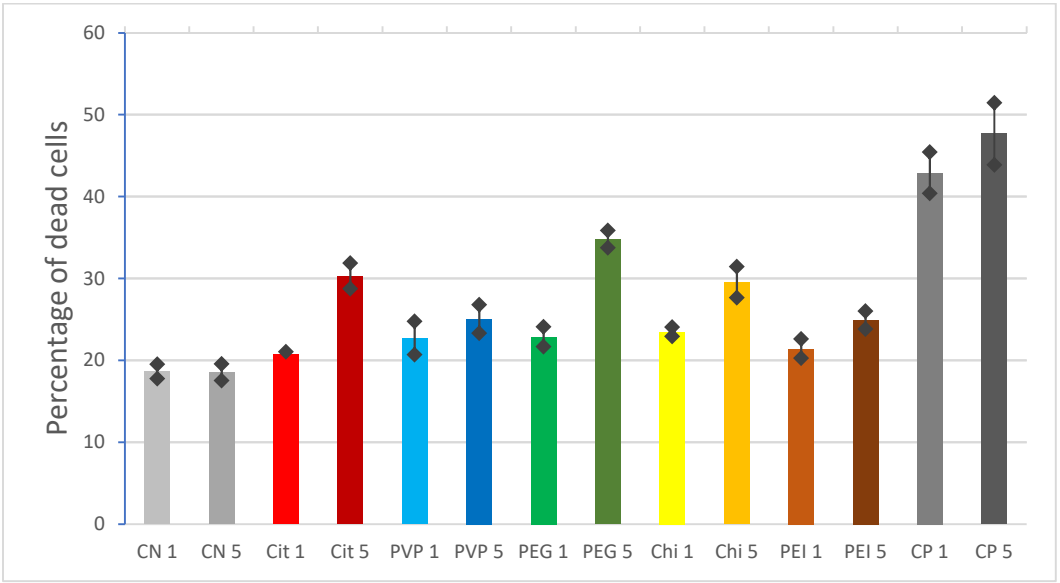

Figure A28.- Confocal microscope results,average and standard error (N=5). Percentage of dead cells after E. coli bacteria has been exposed to Ag NPs solutions for 1 min and 5 min exposure. Longer exposure resulted in higher percentage of dead cells.